

The Geological Society of America
 Special Paper 463
 2010

Structure and $^{40}\text{Ar}/^{39}\text{Ar}$ K-feldspar thermal history of the Gold Butte block: Reevaluation of the tilted crustal section model

Karl E. Karlstrom*

Department of Earth and Planetary Sciences, University of New Mexico, Albuquerque, New Mexico 87131, USA

Matt Heizler

New Mexico Bureau of Geology and Mineral Resources, New Mexico Institute of Mining and Technology, Socorro, New Mexico 87801, USA

Mark C. Quigley†

Department of Earth and Planetary Sciences, University of New Mexico, Albuquerque, New Mexico 87131, USA

ABSTRACT

This paper reevaluates the geometry and processes of extension in the boundary zone between the western Colorado Plateau and the Basin and Range Province. Based on new mapping of extensional detachment faults, restored cross sections, and $^{40}\text{Ar}/^{39}\text{Ar}$ K-feldspar thermochronology, we present an alternative to the previously published model that the Gold Butte block is a tilted 15–18-km-thick intact basement crustal section. Mapping of windows of crystalline basement at 1:12,000 scale delineates a bedding-parallel detachment fault system that parallels the Great Unconformity in the Tramp Ridge block, just north of the Gold Butte block. Above this detachment fault, extensional allochthons containing Upper Paleozoic through Tertiary (>18 Ma) rocks exhibit tilting due to westward translation and tilting. We project this geometry above the Gold Butte block itself based on restoration of slip across the Gold Butte fault. This reconstruction suggests that the detachment system extended over lateral distances of >1000 km², helping define a region of relatively modest extension (~25% for cover; 10% for basement) within the Nevada transition zone between the Colorado Plateau and Basin and Range.

In agreement with previously published mapping and structural cross sections, our restored cross sections suggest that extensional deformation initiated with formation of hanging-wall anticlines above a listric Grand Wash fault system and evolved via a combination of both listric faulting and domino-block translation and tilting. New data presented in this paper document that extension was also facilitated by slip on bedding-subparallel detachment zones in the Bright Angel Shale, along the basement unconformity, and along other zones of weakness, such that the extended

*kek1@unm.edu

†Current address: Department of Geological Sciences, University of Canterbury, Christchurch 8140, New Zealand.

Karlstrom, K.E., Heizler, M., and Quigley, M.C., 2010, Structure and $^{40}\text{Ar}/^{39}\text{Ar}$ K-feldspar thermal history of the Gold Butte block: Reevaluation of the tilted crustal section model, in Umhoefer, P.J., Beard, L.S., and Lamb, M.A., eds., Miocene Tectonics of the Lake Mead Region, Central Basin and Range: Geological Society of America Special Paper 463, p. 331–352, doi: 10.1130/2010.2463(15). For permission to copy, contact editing@geosociety.org. ©2010 The Geological Society of America. All rights reserved.

Paleozoic cover was partly decoupled from less-extended basement. This detachment system ramps down into basement to merge with the South Virgin–White Hills detachment at the west end of Gold Butte, the principal extensional detachment of the region. Our mapping and structural model suggest that movement on these detachment faults initiated at low angle. Further, using the geometry from restored cross sections, we infer that the deepest rocks now exposed in the western Gold Butte block resided at depths of ~4 km below the Great Unconformity (~8 km below the surface) rather than the previously published 15 km below the unconformity (~19 km below the surface). New $^{40}\text{Ar}/^{39}\text{Ar}$ K-feldspar thermochronology from the Gold Butte block, added to a compilation of published thermochronologic data, is used to help evaluate alternative models. K-feldspar multiple diffusion domain (MDD) modeling suggests that rocks throughout all but the westernmost part the block had cooled through 150–200 °C before the Phanerozoic and resided at temperatures <200 °C prior to onset of rapid Miocene extension at 17 Ma. Pre-extensional (pre-17 Ma) 100 °C and 200 °C isotherms were located near the east and west ends of the basement block, respectively. Muscovite, biotite, and K-feldspar from a 70 Ma Laramide pluton deep in the block give $^{40}\text{Ar}/^{39}\text{Ar}$ ages of 70, 50, and 30 Ma, respectively. MDD modeling of K-feldspar from this sample is compatible with cooling the westernmost part of the block from 225 °C to 150 °C between 17 and 10 Ma. Available thermochronology can be explained by either structural model: our model requires pre-extensional geothermal gradients of ~25 °C/km, rather than 15–20 °C/km as previously published.

INTRODUCTION AND GEOLOGIC BACKGROUND

The Gold Butte region of southern Nevada forms part of the transitional boundary zone between the relatively undeformed Colorado Plateau to the east and the highly extended regions of the Great Basin (Fig. 1). This has been a type area for developing and testing models of extensional processes in continental settings. For example, this region was the centerpiece for models of isostatic uplift of footwall blocks during extension (Wernicke and Axen, 1988) and related models for isostatically driven tilting and folding of initially high-angle faults to become low-angle normal faults (Duebendorfer and Sharp, 1998; Brady et al., 2000). This area has also provided an important field laboratory to evaluate the question of whether low-angle faults move at low angle, or are rotated to low angle due to isostatic footwall response (rolling hinge model; Buck, 1988; Wernicke and Axen, 1988) and/or due to progressive domino faulting (Proffett, 1977; Chamberlain, 1983; Axen, 2007). The region has been a test bed for understanding the extent to which thrusts may be reactivated as normal faults (Wernicke et al., 1985; Axen, 1993), and it has spawned diverse models to explain the extensional geometries, for example, N-S shortening synchronous with E-W extension (Anderson and Barnhard, 1993; Anderson et al., 1994) and upper-crustal response to lower-crustal flow (Langenheim et al., 2001).

The central topic of this paper, the Gold Butte block, is one key to resolving these different models. It has been proposed to be a 15–18-km-deep intact crustal section that was initially bounded by steeply dipping normal faults that were tilted to shallow dips due to isostatic uplift resulting from regional detachment faulting (Fig. 2A; Wernicke and Axen, 1988; Fryxell et al., 1992; Reiners et al., 2000; expanded upon herein). This and adjacent parts of

the North and South Virgin Mountains of Nevada (Fig. 1) are segmented into basement-cored crustal blocks by low-angle normal faults and contemporaneous high-angle strike-slip faults (Beard, 1996). The Precambrian-cored blocks have strikingly different geometries. The Gold Butte block exposes a 20-km-wide exposure of Proterozoic basement west of and beneath ~50°E-tilted Paleozoic strata. The dipping strata correlate with nearby flat-lying Grand Canyon successions, and simple restoration of their steep dip has led to the tipped crustal section model (Fig. 2B; Fryxell et al., 1992). On the west edge of the Gold Butte block, and extending to the south and north, there is a low-angle extensional detachment fault system called the South Virgin–White Hills detachment fault (Fig. 1; Duebendorfer and Sharp, 1998), which dies out southward against the Black Mountain accommodation zone (Faulds and Varga, 1998) and correlates northward with the Beaverdam and Snake Range detachments. The trace of this detachment system is just east of the trace of frontal thrusts of the Sevier thrust system (Fig. 1).

North of the Gold Butte basement block, across the Gold Butte strike-slip fault (Fig. 1), the Tramp Ridge and the Lime Ridge blocks are characterized by small basement windows exposed beneath generally E-tilted sections of Paleozoic rocks. Farther north, the Virgin Mountain anticline (VMA of Fig. 1) is a large NE-trending basement-cored uplift (Quigley, 2002; Quigley et al., this volume), and the Beaverdam Mountains expose a small basement block beneath the Beaverdam detachment zone (Fig. 1).

The Gold Butte block has been interpreted to have been uplifted via isostatic uplift of the footwall of the South Virgin–White Hills detachment fault accompanying extensional break-away of Basin and Range blocks from the Colorado Plateau

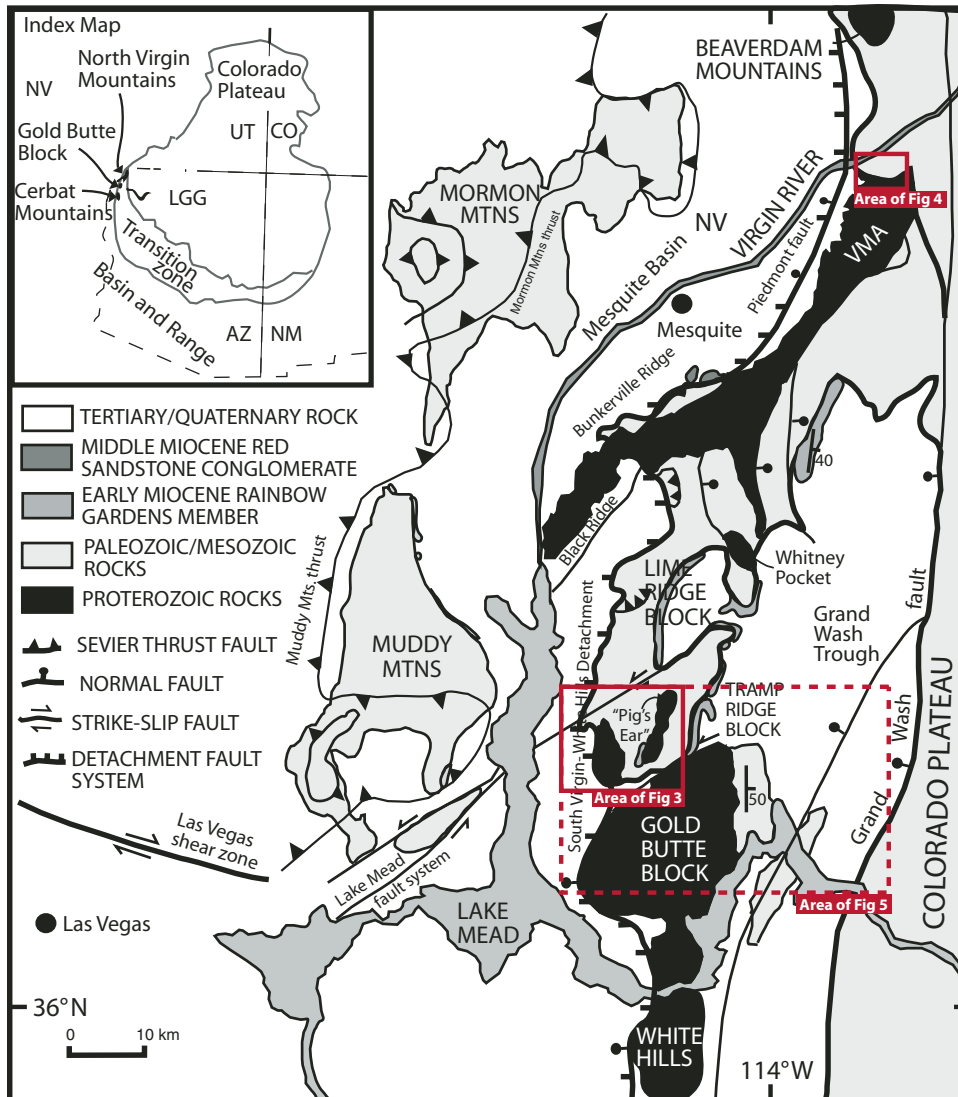


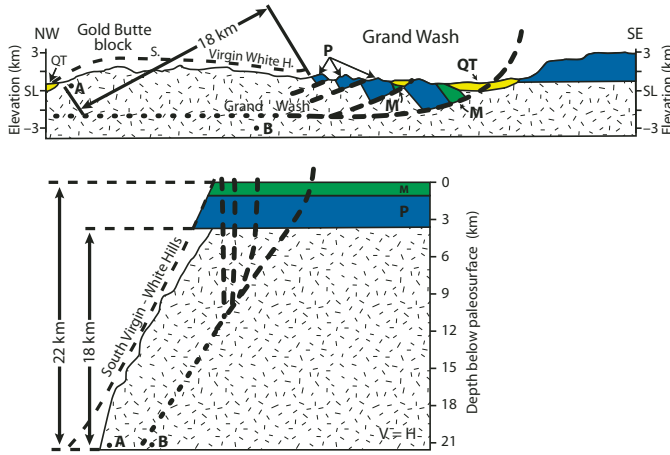
Figure 1. Location map of the Gold Butte block and North Virgin Mountains (adapted from Beard, 1996) showing fault blocks cored by Precambrian basement (black). Inset shows location of Gold Butte and Lower Granite Gorge (LGG) in the context of the transitional boundary zone between the Colorado Plateau and Basin and Range Province. Locations of Figures 3, 4, and 5 are also shown. VMA—Virgin Mountain anticline.

across the Grand Wash fault system (Fig. 2A; Wernicke and Axen, 1988). This model interprets the basement block to expose a 15–18-km-deep crustal depth section that initiated along a subplanar 60°W-dipping normal fault, followed by tilting of the fault and its footwall to the surface due to isostatic effects accompanying progressive extension (Figs. 2A, 2B, and model 1 of Fig. 2C).

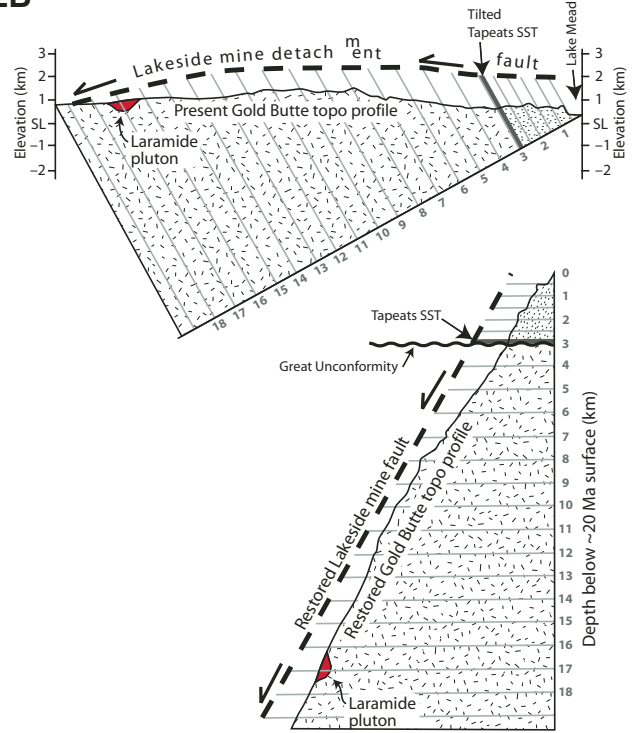
This model has been supported by structural mapping, thermobarometry in basement rocks, and megacryst distributions in Mesoproterozoic granites (Fryxell et al., 1992). More recent mapping of the extensional fault systems of the block has shown a more complex model for the extension (Brady et al., 2000), but the conceptual crustal section model still dominates the literature (e.g., Fitzgerald et al., 2009, p. 28). In this paper, we build on the excellent maps and cross sections of Brady et al. (2000) and expand upon the synchronous slip model involving slip on listric and planar faults by adding evidence for slip on initially subhorizontal detachment faults.

The concept of an intact crustal section extending to middle-crustal paleodepths has led to intensive study of the Gold Butte block using a variety of thermochronometers. These include: (1) fission-track studies on apatite (Fitzgerald et al., 1991, 2009) and zircon (Bernet et al., 2002), (2) (U-Th)/He thermochronology on apatite and titanite (Reiners et al., 2000), and (3) Ar K-feldspar studies (this paper). All data suggest that the Precambrian rocks just under the E-tilted Tapeats Sandstone unconformity at the east end of the block, like rocks in the adjacent Grand Canyon (Kelley et al., 2001; Flowers et al., 2008), record pre-Miocene (pre-extensional) cooling through 70–110 °C. In contrast, rocks at the western end of the block were hotter in the Miocene and give ages consistent with cooling through various closure temperatures (for apatite fission track [AFT], U-Th/He, and Ar) during Miocene extension. The collective data indicate that Miocene extension took place mainly between 17 and 14 Ma (Fitzgerald et al., 1991, 2009; Reiners et al., 2000; Quigley et al.,

2A



2B



2C

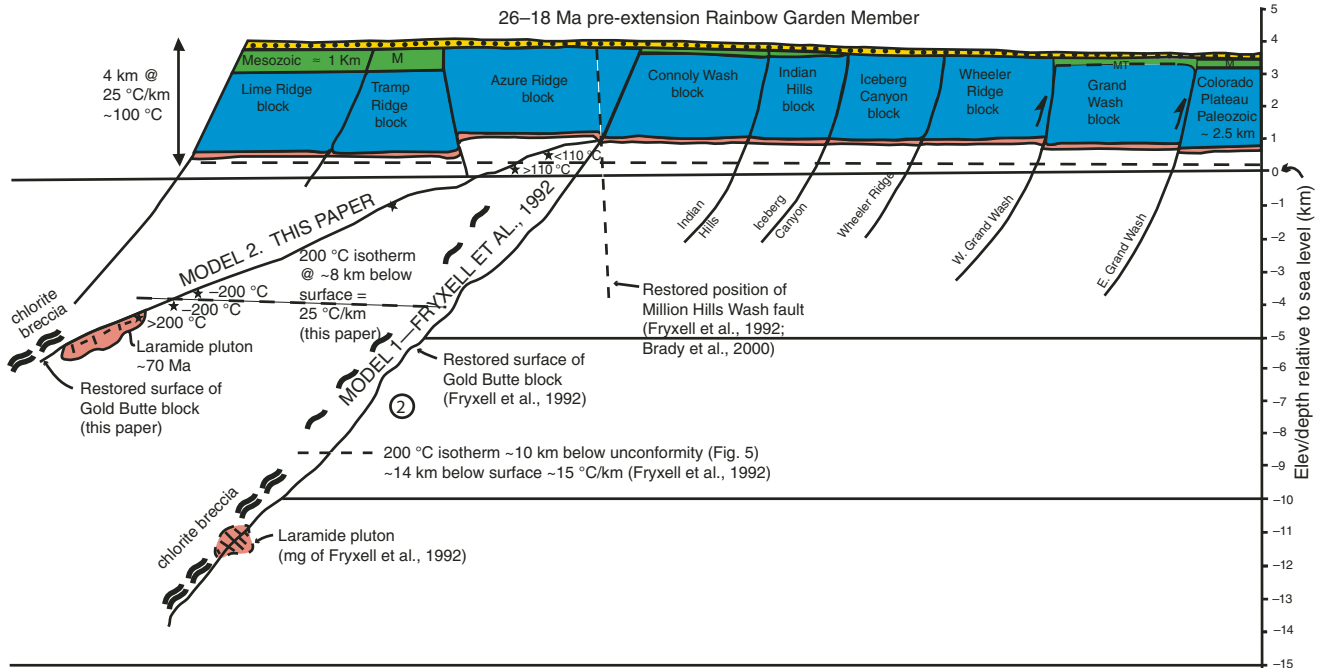


Figure 2. Alternate structural models for the restored geometry of the Gold Butte block. (A) Model 1 from Wernicke and Axen (1988) and (B) model 1 from Fryxell et al. (1992). SL—sea level; SST—sandstone. (C) Alternative models: model 1 (as in A and B) interprets the present surface to be a tilted crustal cross section, the west end of which was exhumed from a depth of ~18 km. Model 2 (this paper) interprets the west end of the present surface to have been exhumed from a depth of ~8 km.

this volume), and the combined data allow well-constrained placement of pre-extensional (pre-17 Ma) 100 °C and 200 °C isotherms (see following discussion).

This paper presents new $^{40}\text{Ar}/^{39}\text{Ar}$ thermochronologic studies of basement rocks in the proposed crustal section at Gold Butte to add to published thermochronologic data. The cooling history of the block is becoming exceptionally well known, but resolving uncertainty about the depth from which exposed crustal rocks were exhumed requires: (1) understanding the geometry and kinematic history of extension (e.g., in restored cross sections), and (2) inferring the geothermal gradient for the pre-extensional and extensional tectonic regimes, which are the subjects of this paper. Published estimates for the geothermal gradient in the region range from ~15 °C/km (Fryxell et al., 1992), to 20 °C (Reiners et al., 2000; Fitzgerald et al., 2009) to 25 °C/km (this paper).

Large-magnitude extension was mostly over in this area by ca. 14 Ma (Beard, 1996; Brady et al., 2000). However, continued 100-m-scale slip on the Wheeler and other normal faults is now well documented by offset of the 6 Ma Hualapai Limestone and accompanying formation of a hanging-wall anticline in this unit and in slightly younger (4.7 Ma) basalts at the mouth of Grand Wash (Howard and Bohannon, 2001; Karlstrom et al., 2008). The locus of post-6 Ma extension in the broad transitional domain between the Colorado Plateau and Basin and Range has migrated eastward into the Colorado Plateau to the currently active Hurricane and Toroweap faults (Brumbaugh, 1987; Jackson, 1990; Karlstrom et al., 2007, 2008). The slip history on the combined Wheeler-Hurricane-Toroweap faults over the last 6 m.y. has involved formation of hanging-wall anticlines above listric faults, as well as uplift of the Colorado Plateau relative to the Basin and Range by 750–900 m (Karlstrom et al., 2007, 2008). These new data supporting active listric faulting and the process of formation of hanging-wall anticlines are incorporated into our model for the geometry and history of Miocene faulting across the Gold Butte block.

EVIDENCE FOR BEDDING-SUBPARALLEL MIOCENE EXTENSIONAL DETACHMENT FAULTS

Detailed mapping (scale 1:12,000) of the Tramp Ridge area in 1998–1999 by the combined Massachusetts Institute of Technology (MIT) and University of New Mexico (UNM) advanced field camps is shown in Figure 3A and superimposed on thermal infrared multispectral scanner (TIMS) images in Figure 3B. TIMS images were processed following methods outlined in Hook et al. (2005). Because of the sensitivity of the thermal infrared part of the spectrum to silicate mineralogy, these images do an excellent job of distinguishing silicate compositions in basement and cover sequences. Companion AVERIS (Airborne Visible/Infrared Imaging Spectrometer) images were used to distinguish limestones from dolomites and further help delineate units. These images, confirmed by detailed mapping, reveal a persistent association of small outcrops of the Tapeats

Sandstone (brightest spectral response due to high-SiO₂ content and red color in Fig. 3B) adjacent to Proterozoic basement over a wide region in Precambrian-cored domes (West Dome and Pig's Ear of Fig. 3A) in the Tramp Ridge block.

The basement windows of the Tramp Ridge block are a series of doubly plunging anticlines that are rimmed semi-continuously by fragments of Lower Paleozoic strata (Figs. 3A and 3B), which are variably attenuated, but in correct stratigraphic order, and are locally in depositional contact with basement. In the thickest sections (Fig. 3A), the Tapeats Sandstone–Bright Angel Shale section is close to its depositional thickness, but in most areas, the section is thinned. In many segments of the contact, the Tapeats Sandstone is missing entirely, and the Bright Angel or Muav Formations rest on basement. Basement rocks near the contact are locally deeply weathered, similar to outcrops of the Great Unconformity in the Colorado Plateau, and are locally cataclastic (e.g., Lime Wash of Fig. 3). Tapeats Sandstone outcrops occur on both east and west sides of the antiformal windows (Fig. 3). Thus, our mapping suggests that the basement domes are mini-core complexes or domelike features and are not fundamentally defined by N-S fault zones bounding their west sides.

These relationships indicate that a complex low-angle fault zone anastomoses along the Great Unconformity and adjacent bedding planes, mainly following the weak Bright Angel Shale. Because Lower Paleozoic strata are parautochthonous relative to basement, and the Lower Paleozoic strata have low to moderate dips all around the domal outcrops, we infer that the basement sections themselves are not strongly tilted. In contrast, carbonate units above the Bright Angel Shale are commonly in fault contact with younger units and are dominantly E-tilted, nose-down, against the footwall rocks. Thus, overlying carbonate units are tilted and have been translated westward relative to basement rocks along a detachment fault system that generally follows the Great Unconformity and that is broadly folded above the basement windows.

An outcrop-scale analog for this geometry (Figs. 4A and 4B) shows tilted and extended domino blocks of Tapeats Sandstone riding on a detachment fault that is subparallel to the Great Unconformity in the North Virgin Mountains (Quigley et al., this volume). Although this outcrop example is north of the Gold Butte area, and opposite in slip direction, it displays features illustrative of the bedding-parallel detachment faults in both areas. Semi-regularly spaced domino blocks of Tapeats Sandstone have been tilted by movement along this low-angle fault (Fig. 4B). Small basement domes form in response to space problems caused by domino-block rotation (Figs. 4B and 4C), perhaps analogous to the larger domes seen in the Gold Butte block.

The detachment fault in the Virgin Mountains is made up of several components. Below the domino blocks, there is a zone (<1 m thick; Figs. 4B, 4C, and 4D) of white cataclastic breccia made up of blocks and grains of Tapeats Sandstone. Below this, the detachment itself is defined by a several-centimeter-thick zone of red silty cataclasite (Figs. 4D–4F) that appears to

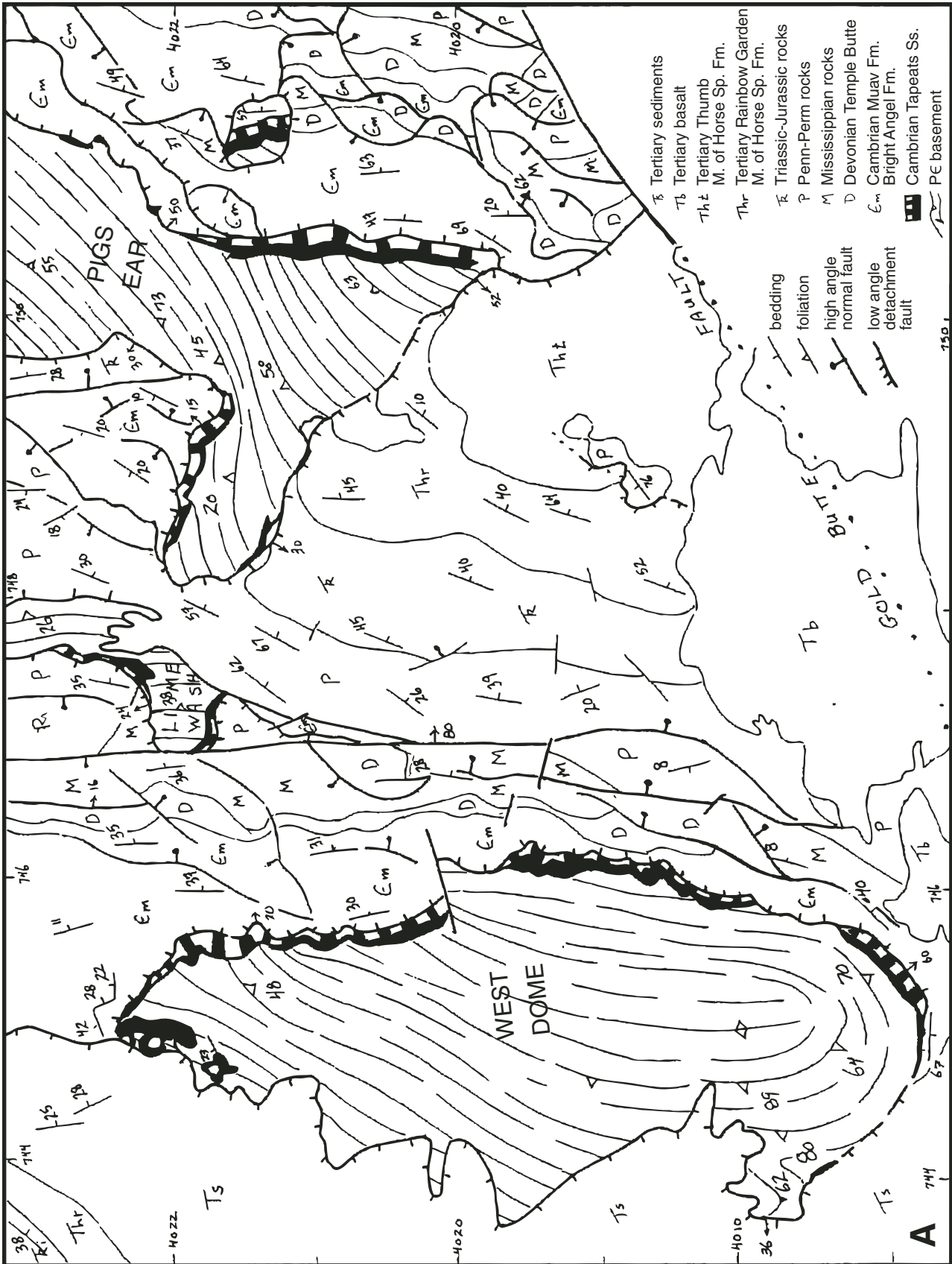


Figure 3 (on this and following page). (A) Simplified geologic map of the Tramp Ridge block showing basement-cored domes rimmed by a detachment fault system; generalized from 1:12,000 mapping from the Massachusetts Institute of Technology–University of New Mexico (MIT-UNM) field camps with depiction of small-offset normal faults in the Paleozoic rocks simplified from new mapping, Brady et al. (2000), and Beard et al. (2007).

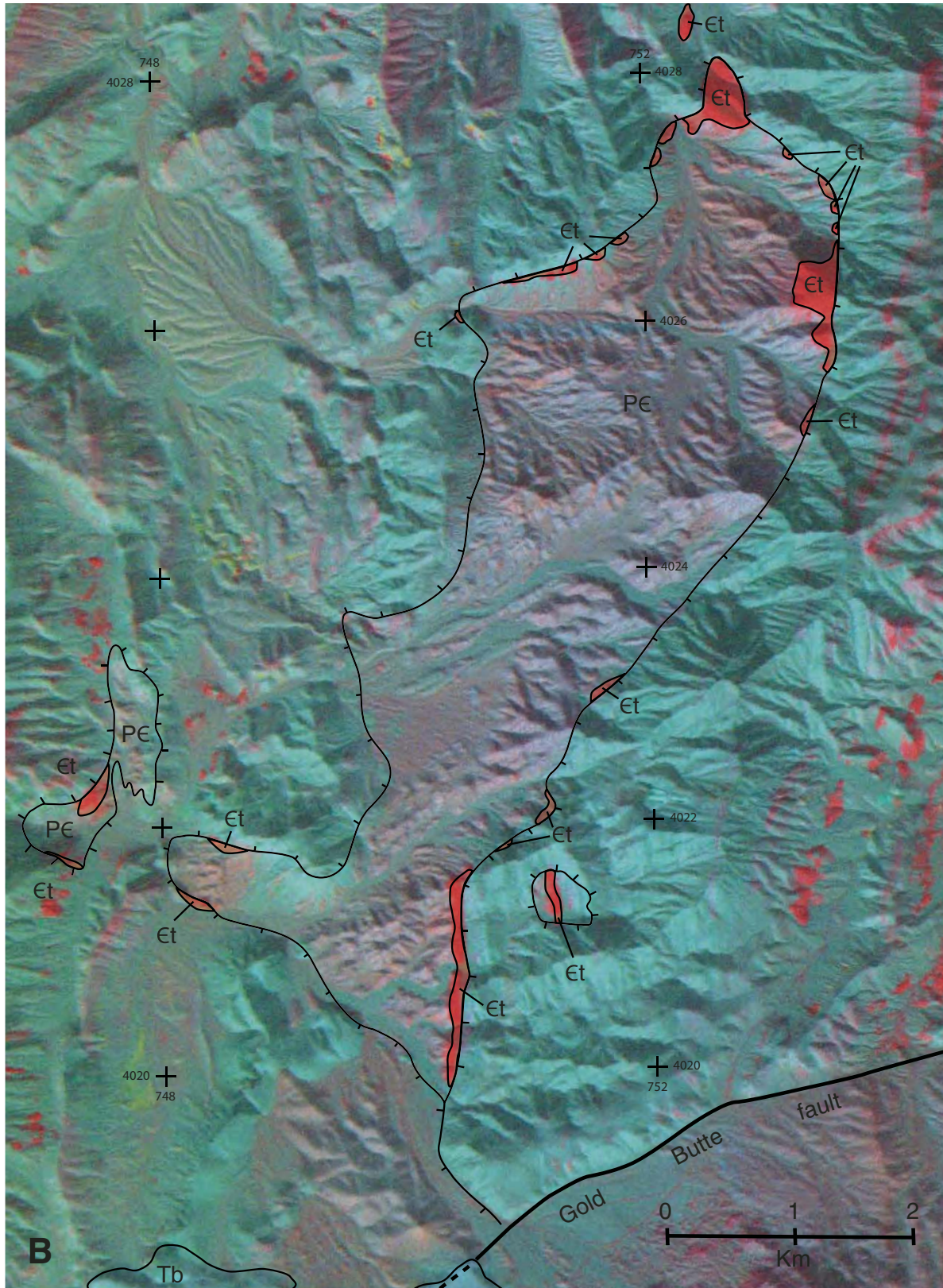
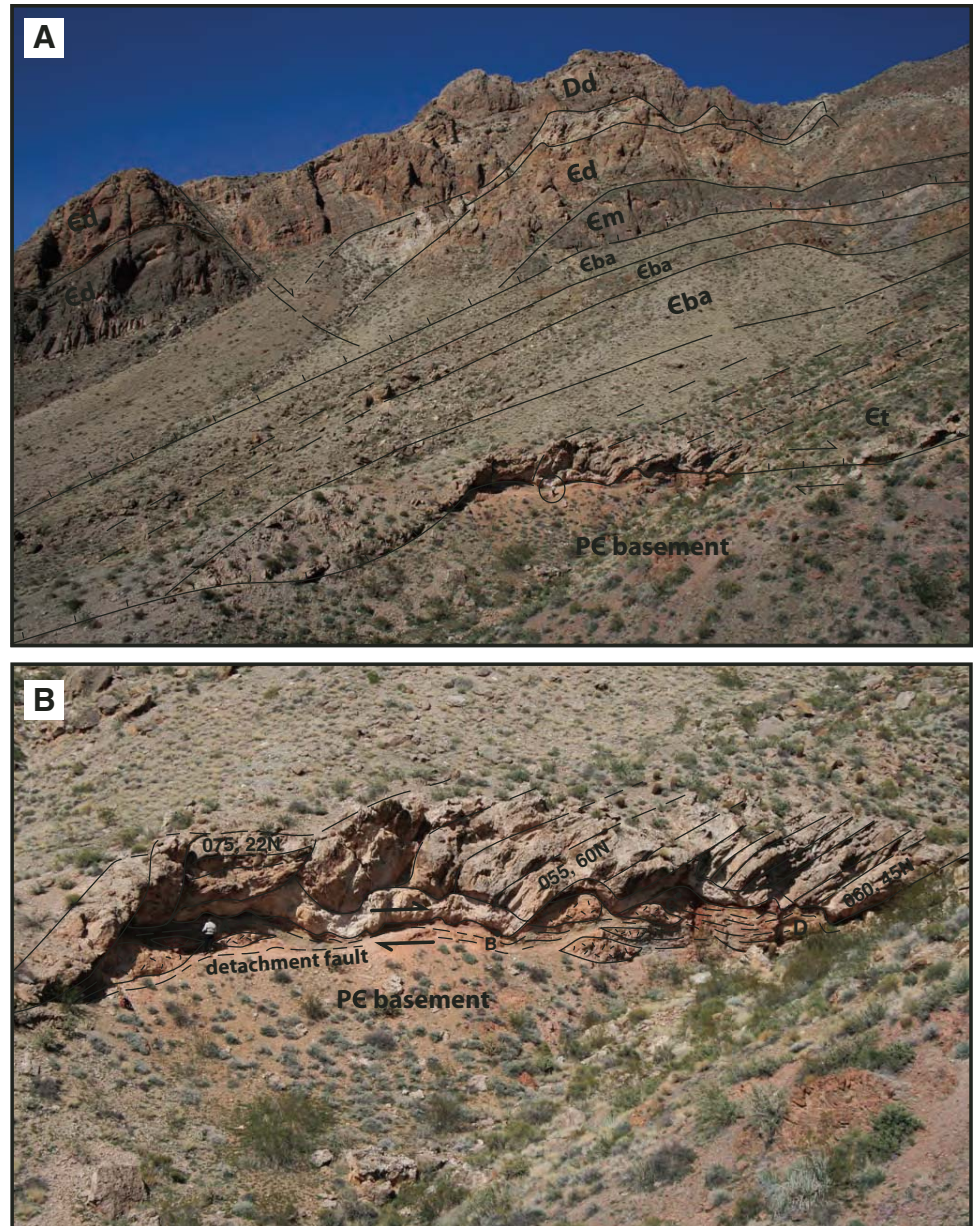


Figure 3 (continued). (B) Thermal infrared multispectral scanner (TIMS) image of the Pigs Ear basement-cored dome with detachment fault system extrapolated north of the map area of A based on only local preservation of Tapeats Sandstone at the basement-cover contact, as well as the presence of attenuated Tapeats Sandstone slivers on both east and west margins of the dome.

Figure 4 (on this and following page). Detachment fault geometry. (A) View, looking northeast, is cliff of Paleozoic carbonates on the north side of the Virgin Mountains, just west of Mesquite, Nevada. Note truncation of Muav Limestone on a detachment fault at the top of the Bright Angel Shale, and location of the tilted blocks of Tapeats Sandstone riding on a detachment that follows the Great Unconformity. Person for scale. (B) Outcrop-scale example of the low-angle detachment fault system; from bottom to top: cataclastically deformed basement (lines), including boudins of pegmatite (hatchers), breccia of Tapeats Sandstone (white), and tilted domino blocks of Tapeats Sandstone.



be derived from fine-grained layers in the Tapeats Sandstone. Basement rocks below the detachment are characterized by a several-meter-wide zone of cataclasite, with discrete planar ultracataclasites marking faults (Fig. 4E), fractured and boudinaged pegmatites (Figs. 4B and 4C), and brittle/ductile features such as S-C fabrics in anastomosing cataclastic foliation (Figs. 4E and 4F). In the nooks between domino blocks, basement fabric can be domed, and straight short-cut faults formed during the progressive deformation (Fig. 4C).

In the Gold Butte area (Figs. 3 and 5), and at a range of scales, Paleozoic through Tertiary strata in the hanging wall of the domal detachment faults in the Tramp Ridge block are also interpreted as extensional allochthons, with beds commonly dip-

ping 40° – 60° E, against the detachment. In the Tramp Ridge cross section of Brady et al. (2000; A–A' of Fig. 6C), hanging-wall blocks are internally deformed but essentially represent several large E-tilted dominos that were translated westward several kilometers on the basal detachment (Fig. 6). Normal faults in the dominos are higher angle (30° – 60°) and merge downwards with and locally crosscut the detachment. At the west edge of the anticlines, the areas where the domino faults merge with the detachment (Figs. 3 and 6), interaction of the domino faults and detachment produce complex “chaos” structures up to hundreds of meters thick. Basement anticlines (labeled 1–7 in Fig. 6) have a fairly regular geometry and spacing, due to tilting of the domino blocks. East limbs of the domal anticlines, although brecciated

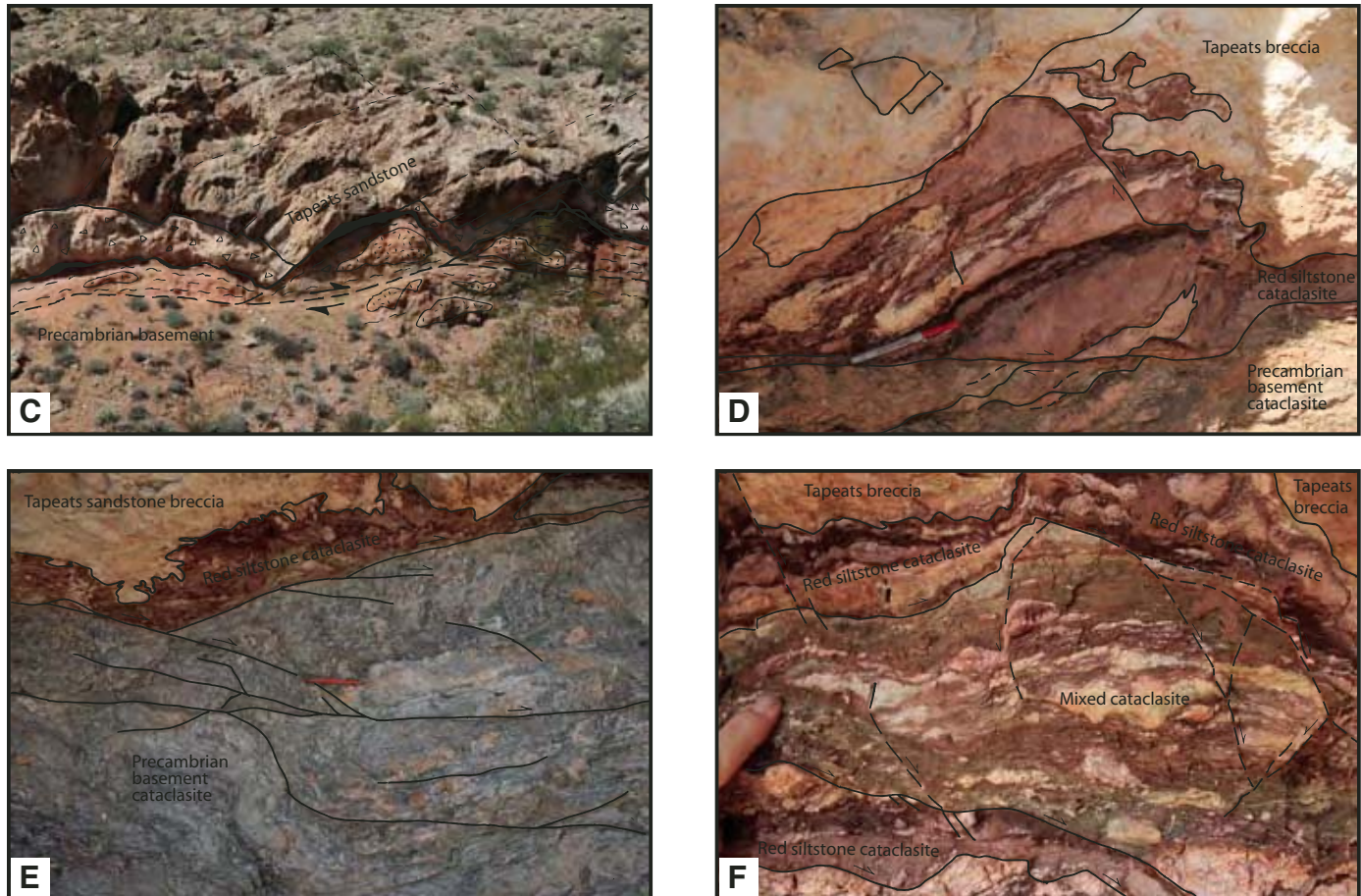


Figure 4 (*continued*). (C) Detail of the detachment fault showing domino blocks, breccia zone of crushed Tapeats Sandstone, a red (silty) cataclasite along the detachment fault, and anastomosing cataclastic foliation and faults in the Precambrian basement. (D) Synthetic (top-south) normal faults in red cataclasite and fault shortcut between the bases of two domino blocks. (E) Red cataclasite at detachment, and cataclastic foliation and ultracataclasite fault zones in basement rocks. (F) Close up of detachment fault showing brittle and brittle-ductile deformation in the basement rocks.

and attenuated, are generally less complex and have less attenuation of Lower Paleozoic strata in the area of Figure 3. However, mapping indicates that the basement-cover contact shows attenuation of Lower Paleozoic units and the presence of a regional low-angle detachment, even at the east end of the Gold Butte block, in the Indian Hills (Fig. 7B), and the Azure Ridge blocks (see Fig. 5 for locations).

Restoration of the cross section (Figs. 6A and 6B) suggests that ~25% (<10 km) of E-W extension of Upper Paleozoic rocks (Y to Y') is accommodated by a combination of mechanisms, including tilting and internal faulting in dominos (in agreement with Brady et al., 2000). However, because of slip on the unconformity and hanging-wall flexure, we infer that the percent of extension of the basement in this cross section (Z to Z') is only ~10% (Fig. 6) and is accomplished mainly on the deeply penetrating master listric faults. In contrast, cross sections by Brady et al. (2000) showed a similar magnitude of extension for both basement and cover.

RELATIVE IMPORTANCE OF LISTRIC VERSUS PLANAR FAULTS

Model 1 of Figure 2 involves a set of subplanar, 60°-dipping, deeply penetrating normal faults that get tilted by isostatic doming and progressive extension. This model assumes that the deformation can be restored by a simple untilting of the ~50°E-dipping Paleozoic strata to horizontal. However, this structural model would need to be modified if the cover were detached from the basement and/or if some portion of the tilt of the Paleozoic strata were due to hanging-wall flexure (Fig. 7A).

Curved contacts for Paleozoic strata observed in the Wheeler Ridge and Azure Ridge blocks support the interpretation that listric master faults may bound parts of the extensional allochthons (Figs. 7A and 7B; in agreement with Brady et al., 2000). Hanging-wall flexure is also observed for deformation of the Hualapai Limestone and 4.7 Ma basalts in the hanging wall of the Wheeler fault, with offset of ~450 m, flexure wavelength

Figure 5. Map of Gold Butte block modified from Brady et al. (2000) and new mapping (this paper); thermochronologic data are from Fitzgerald et al. (1991, 2009); Reiners et al. (2000), and this paper. Cross sections A–A' and B–B' are modified from Brady et al. (2000); cross section C–C' (modified from Fryxell et al., 1992) shows the paleodepths inferred in the Fryxell et al. (1992) model (model 1 of this paper). Locations of Figures 3 and 7 are shown.



of ~7 km, and hanging-wall dips of ~15° formed in the last 6 m.y. of moderate extension (Howard and Bohannon, 2001). Similarly, differential incision rate data from the Grand Canyon show that extension across the neotectonic Toroweap and Hurricane faults in the last 600 k.y. involved ongoing formation of a hanging-wall flexure above listric faults (Karlstrom et al., 2007, 2008). Thus, using time-for-space comparisons, Figure 6 incorporates listric faults for the main block-bounding structures and envisions that an important component of the dip of Paleozoic strata is due to hanging-wall flexure. If this is correct, most of the basement of the Gold Butte block should be less-rotated than the 50° dip of the Paleozoic rocks in the Azure Ridge block, compatible with the evidence for slip of cover allochthons above less-extended basement.

GOLD BUTTE STRIKE-SLIP FAULT

The Gold Butte fault is one of a family of NE-striking strike-slip faults related to the sinistral Lake Mead fault zone (Fig. 1; Bohannon, 1979). The kinematic significance of this fault has been controversial, and there is disagreement regarding the sense and magnitude of strike slip and the relative importance and relative timing of normal and strike-slip faulting (Beard, 1996). Our mapping supports the interpretation that the Gold Butte fault moved simultaneously with the major domino-bounding normal faults (Beard, 1996) and is a transfer fault (transtensional lateral ramp) related to the South Virgin–White Hills detachment, with substantial slip at its west end and diminishing slip toward its east end.

Hence, we infer that styles of extension may be similar across it. This is reinforced by the scoop-shaped bend in the strike-slip fault into the “Rainbow Ridge” fault, which bounds the eastern of the two domino blocks (Fig. 5).

In this region, Figure 5 shows a modification to the Beard et al. (2007) compilation. Proterozoic basement rocks with undisrupted foliation trends are exposed across the northeastern end of the Gold Butte fault, suggesting that the main slip has been transferred to the Rainbow Ridge extensional fault at this point. Synorogenic conglomerates and megabreccias of the synextensional Thumb Member (16–14 Ma) here unconformably overlie basement rocks and are themselves weakly E-tilted, indicating that the combined extensional–strike-slip system denuded a portion of basement during deposition of the Thumb Member. The abundance of Precambrian clasts in the mixed-clast conglomerate and an unroofing sequence in the Gold Butte conglomerate suggest that Paleozoic rocks, then crystalline basement of the

Gold Butte block, were being erosionally denuded during left-lateral and north-side-down movement on the Gold Butte fault ca. 17–15 Ma, before much of the E-tilting occurred in the Tramp Ridge area. Mullions and slickenlines on the Gold Butte fault rake 10°SE on the steeply NW-dipping fault planes, compatible with a sinistral oblique slip (minor south-side-up component). This left-lateral interpretation is in agreement with Longwell et al. (1965), Bohannon (1984), Beard (1996), and Brady et al. (2000). South-side-up components of slip are also indicated by an overturned syncline of Tertiary strata north of the fault. An alternate interpretation (Fryxell et al., 1992), that the fault is a right-lateral tear in the hanging wall of the South Virgin–White Hills detachment, is not supported by our mapping, which indicates that the apparent dextral bend of the Rainbow Garden Member of the Horse Springs Formation is not a drag feature, but instead is related to the scoop-shaped links between extensional and strike-slip faults.

Thus, we interpret the Gold Butte block to have a similar structure as the Tramp Ridge block and hence to also contain relatively untilted basement. To reconstruct regional cross sections, we infer that the Gold Butte block is a more deeply eroded analog of the Tramp Ridge block, where a basement-cover detachment fault has been eroded through to expose the present level of the Gold Butte block. Paleozoic strata preserved at the east end of the Gold Butte block (Azure Ridge) are interpreted to be part of a hanging-wall anticline (Fig. 6B), such that dips may have decreased westward (Brady et al., 2000) rather than continuing at this same dip for many kilometers (cf. Fryxell et al., 1992; Reiners et al., 2000). In support of this idea, the Lower Paleozoic rocks in the Azure Ridge and Indian Hills blocks, in the eastern Gold Butte block (Fig. 5), are similar to E-dipping limbs of the anticlinal windows in the Tramp Ridge block in showing attenuation of strata and presence of a detachment at several stratigraphic levels, from the Bright Angel Shale to the Great Unconformity. The tilted crustal section model (model 1 of Fig. 2) implies a different style of extension for the Tramp Ridge block relative to the adjacent Gold Butte block, which seems difficult to justify over such short length scales. Hence, in our interpretation, the Gold Butte basement block (cross sections B and C of Fig. 5) is restored below the Tramp Ridge cross section (cross section A of Figs. 5 and 6) to present a composite cross section (Fig. 6C).

In the restored section (Fig. 6A), the Gold Butte block may have been overlain by a slightly thinner section of Paleozoic rocks than the areas farther north prior to extension. This is suggested by paleogeographic reconstructions of the N-tilted and Paleozoic sedimentary succession that become erosionally beveled to lower stratigraphic levels southward due to uplift of the Laramide-aged Kingman highlands (Beard, 1996). In support of this model, pre-extensional rocks of the Rainbow Gardens Member of the Horse Springs Formation rest atop Permian Kaibab in the Azure Ridge block, whereas Triassic rocks are preserved under the Rainbow Gardens Member in the Tramp Ridge and Lime Ridge blocks (Fig. 6A). Figure 6A also suggests that some of the master extensional faults (Wheeler, Grand Wash, and Hurricane faults) may have reactivated Laramide reverse faults.

Figure 6. (A) Pre-extension (ca. 20 Ma) stratigraphy showing west-thickening Paleozoic rocks (P), fault-controlled thickness variation in Mesozoic rocks (M), hypothetical Laramide reverse faults and monoclines, thin pre-extensional 26–18 Ma Rainbow Garden Member (T), and estimated positions of 100 °C and 200 °C isotherms relative to surface that now forms the Gold Butte block. Major fault names and names of prominent ridges of tilted strata (from Fig. 5) are shown. (B) Early stages of extension (~10%) take place via slip on master listric faults, formation of hanging-wall anticlines, and domino block rotation facilitated by slip on weak bedding planes (e.g., Great Unconformity); basement culminations 1–7 are labeled (locations also shown in Fig. 5). (C) Present-day cross section constructed by stacking three cross sections (A, B, C; locations shown in Fig. 5; modified from Brady et al., 2000; Fryxell et al., 1992) and interpreting these as progressively deeper erosional cuts into the Gold Butte block. Thermochronology controls data points as in Figure 5 and isotherms as described in the text. Laramide pluton is shown at the surface near the west end of the Gold Butte block.



EVIDENCE FROM PROTEROZOIC ROCKS

Fryxell et al. (1992) presented several lines of evidence in support of the hypothesis that the Gold Butte Proterozoic rocks represent a single tilted crustal section that extends from the Great Unconformity (beneath Azure Ridge on the east) to paleodepths of ~13–15 km below the unconformity. A brittle-ductile shear zone and associated chlorite breccia (Lakeside Mine of Fryxell et al., 1992; South Virgin–White Hills detachment of Duebendorfer and Sharp, 1998) form the west edge of the Gold Butte block. To help with the following discussion, Figures 2B and 5 (cross section C–C') show a scale bar for model 1: pre-Miocene paleodepth is labeled on cross section C according to the tilted crustal section model (model 1 of Fig. 2).

One line of evidence for the tilted crustal section model was thermobarometry of Proterozoic rocks. Fryxell et al. (1992) reported that Proterozoic rocks directly beneath the unconformity gave pressures of ~300 MPa, whereas those ~10 km deeper gave pressures of 600 MPa. This was interpreted as a frozen-in Proterozoic depth gradient that had been up-ended in the Tertiary. However, this interpretation was based on just three of four samples analyzed. One problem with the interpretation of these data is the absence of pressure-temperature (*P-T*) path information in rocks that we know to have complex Proterozoic *P-T* history. Thermobarometry studies in the adjacent Grand Canyon basement show evidence for decompression from 600 to 300 MPa during the 1.7–1.67 Ga orogenic event (Williams and Karlstrom, 1997; Karlstrom et al., 2003; Dumond et al., 2007). Similar results were reported by Duebendorfer et al. (2001) from basement rocks of the nearby Cerbat Mountains (Fig. 1). Similarly, the depth significance of the apparent trend of increasing temperature toward the west (Fryxell et al., 1992, Fig. 8C) is called into question by observed large lateral temperature gradients in basement of the Colorado Plateau, which are interpreted to be due to pluton-enhanced metamorphism at constant pressure (Ilg et al., 1996; Williams and Karlstrom, 1997; Dumond

et al., 2007). Without more comprehensive metamorphic analysis involving relative thermobarometry from similar rock types, compositional maps of metamorphic minerals, and *P-T* path information (Dumond et al., 2007), it is unclear if the data presented by Fryxell et al. (1992) represent different parts of such a decompression *P-T* path versus different locations within a depth section. If all four of their samples are considered, the disagreement in estimated pressures between two samples from similar distance below the unconformity (400 versus 600 MPa) is difficult to explain using the uniformly tilted crustal section model but would be compatible in terms of preservation of two different parts of the Proterozoic *P-T* path.

The application of Al-in-hornblende barometry to the 1.4 Ga plutonic rocks shows ~9 MPa/km westward pressure increase (~5 km depth increase over 20 km) rather than the 27 MPa/km (~1 km) postulated in model 1 (Brady, 2005). This may reflect late Precambrian tilting following intrusion of the Mesoproterozoic granites and prior to Phanerozoic deposition (as interpreted by Brady, 2005), but this is counter to regional models for isobaric crustal sections preserved in the Grand Canyon region by 1680 Ma (Karlstrom et al., 2003; Dumond et al., 2007; Williams et al., 2009). Alternatively, these data seem in closer agreement with our suggested paleodepth for the western edge of the block as ~4–5 km below the Paleozoic unconformity. At present, the combined thermobarometry data are ambiguous and do not strongly support one model over the other.

The Gold Butte block contains the Gold Butte granite, a 1.45 Ga pluton (Silver et al., 1977) that is similar in composition and texture to the ca. 1.4 Ga A-type plutons that perforate many regions of the American Southwest. Fryxell et al. (1992) mapped variations in size and density of K-feldspar megacrysts as a possible proxy for depth and reported that phenocryst abundance increases toward the Paleozoic unconformity. They concluded that phenocrysts floated upward within a 10–12-km-thick, now-tilted, magma chamber. However, the physical basis for this inferred phenocryst zonation is questionable; it is not clear if K-feldspar megacrysts are denser or less dense than surrounding magma. Also, intrusion of most of the 1.4 Ga plutons in the region involved sheet-like geometry, multiple intrusions, complex emplacement processes, and synorogenic character (Kirby et al., 1995; Duebendorfer and Christensen, 1995; Nyman and Karlstrom, 1997), so we question the use of megacryst patterns as a reliable proxy for depth in the pluton.

⁴⁰Ar/³⁹Ar Age Spectrum Results

As summarized already, several thermochronology methods have been applied to the Gold Butte tilted section. Previously published ⁴⁰Ar/³⁹Ar data focus on muscovite, for which Reiners et al. (2000) demonstrated an age decrease from 1374 to 90 Ma from east to west across the block. For context, geologic data indicate that rocks near the unconformity cooled to surface temperature (~10 °C) before the deposition of the Cambrian sedimentary section (before ca. 530 Ma). Rocks farther west (deeper)

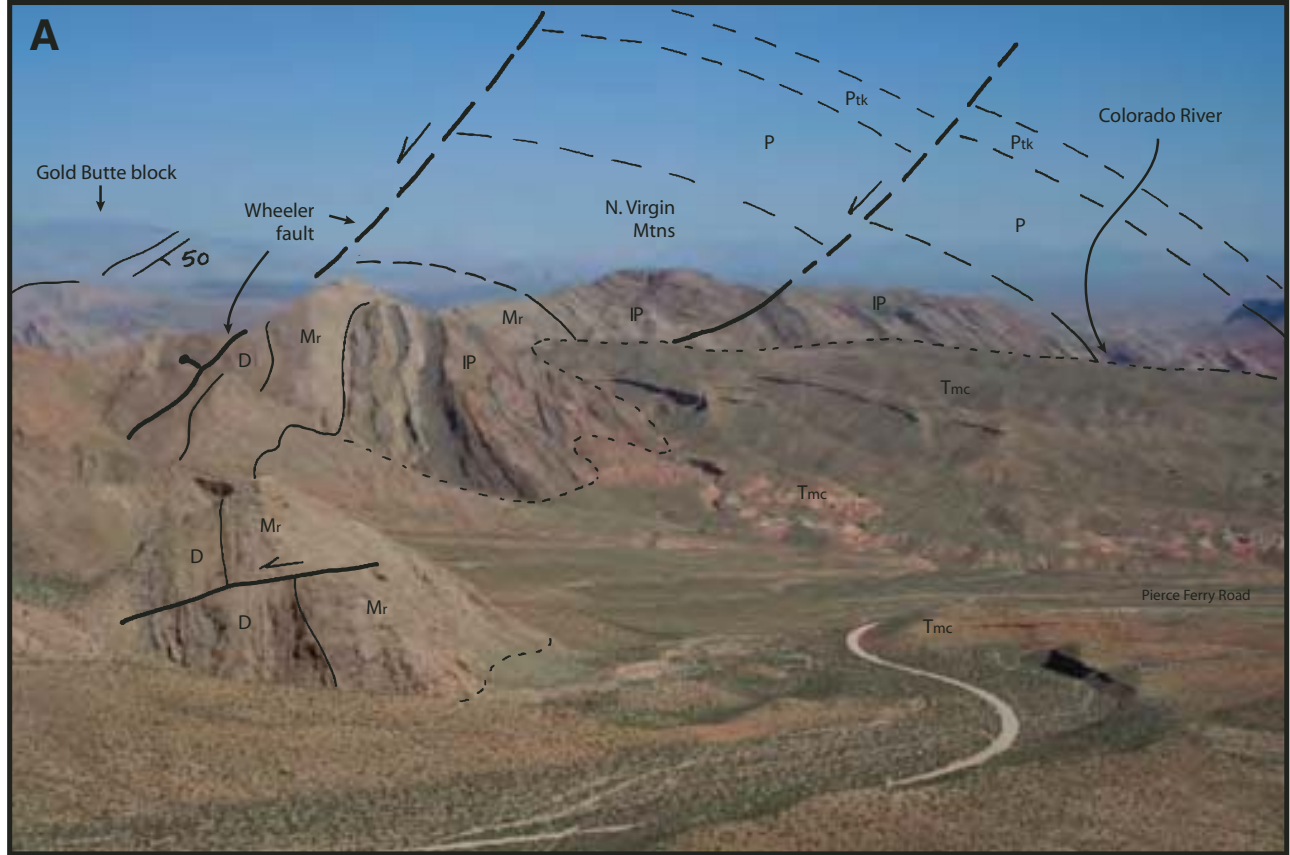


Figure 7. (A) Faulted hanging-wall anticline in Upper Paleozoic rocks of the Wheeler Ridge block formed in hanging wall of Grand Wash fault; see Figure 5 for location. D—Devonian Temple Butte Formation, Mr—Mississippian Redwall Limestone, IP—Pennsylvanian Supai Group, P—Permian rocks, Ptk—Permian Toroweap and Kaibab Formations, Tmc—Tertiary Muddy Creek Formation; Gold Butte block and North Virgin Mountains in distance. (B) Complex hanging-wall anticline in the Indian Hills block, just west of Iceberg Canyon at the southeast edge of the Gold Butte block (see Fig. 5 for location), view looking north. Lower Paleozoic section in right center has Tapeats Sandstone (Ct) and Bright Angel Shale (Cba) above the basement unconformity along parts of the east edge of the Gold Butte block; dotted lines are carbonate markers in the Bright Angel Shale. Locations marked “X” are positions where thin slivers of Tapeats Sandstone and Bright Angel Shale are preserved along the domed Indian Hills detachment fault system that partly follows the unconformity, similar to basement-cored domes of the Lime Ridge block. Fifteen-degree W-dipping Iceberg Canyon fault, mapped by Longwell (1936, 1945) in the west wall of Iceberg Canyon, is now concealed by Lake Mead.



in the block, which are hypothesized to have resided at depths of 15–18 km in the crust, should have cooled slowly as they were erosionally unroofed between 1.45 Ga and Cambrian time. Phanerozoic deposition of 3–4 km of sediments should then have elevated temperatures by ~100 °C before rapid Miocene cooling due to extensional unroofing.

Our new $^{40}\text{Ar}/^{39}\text{Ar}$ data concentrate on the utility of K-feldspar thermochronology; however, hornblende, muscovite, and biotite were also analyzed. Figure 8 displays the new data as age spectra, and sample locations are shown in Figure 5. The argon isotope data are tabulated in Appendix 1,¹ where full analytical details are also provided. Appendix 1 also presents the multiple diffusion domain (cf. Lovera et al., 1989) thermal modeling results for KGB99-1, 16, 27, and 32a but not for KGB99-34 due to the age spectrum complexity (Fig. 8E). Two hornblende results yielded ages of 1613 ± 2 Ma and 1369 ± 6 Ma for KGB99-16 and KGB99-34, respectively (Figs. 8B and 8E). KGB99-16 is a Paleoproterozoic granitoid based on the hornblende result. It is noted that the hornblende spectrum is somewhat complex, and we followed the method of Schneider et al. (2007) in choosing the oldest steps that correspond to a constant K/Ca value to obtain a cooling age. The younger hornblende from KGB99-34 is from the Mesoproterozoic Gold Butte granite and has a fairly well-behaved age spectrum indicating cooling through ~500 °C at ca. 1370 Ma.

Biotite spectra are variably complex and show total gas ages (TGA) decreasing with structural depth. KGB99-16 biotite yields a generally flat spectrum and a plateau age of 1424 Ma, whereas deeper samples from KGB99-27 and KGB99-34 demonstrate likely signs of long-term crustal residence near their argon clo-

sure temperature. KGB99-27 has a climbing spectrum, with several steps yielding apparent ages between 1200 and 1300 Ma and a TGA of 1153 Ma (Fig. 8D). The complex spectrum from KGB99-34 has a shape very similar to those shown by Lo and Onstott (1989) to indicate chlorite alteration, and we do not assign thermochronologic significance to this result, but note that it has a relatively young TGA that is consistent with its deeper structural position. A single Precambrian muscovite was dated from pegmatite KGB99-25, and it yields a very flat spectrum with a plateau age of 1347 ± 1 Ma (Fig. 8C).

The K-feldspars from the Precambrian rocks have total gas ages that decrease with paleodepth and have age spectra that yield age gradients resultant from argon loss that is caused by a protracted thermal history (Fig. 8). KGB99-16 is oldest and reveals an age gradient from ca. 1000 to 1345 Ma that is in slight contrast to KGB99-1, which has an age gradient from ca. 600 to 1300 Ma (Figs. 8A and 8B). Like most K-feldspars, low-temperature heating steps that correspond to duplicate laboratory temperatures show a characteristic old and young age oscillation that may correspond to excess ^{40}Ar trapped in fluid inclusions that decrepitated upon heating during the first replicate temperature (e.g., Harrison et al., 1993). In marked contrast to the structurally higher samples, KGB99-27 shows a significant part of its spectrum with Phanerozoic ages (Fig. 8D). This sample has minimum ages of ca. 30 Ma that climb steadily to ca. 900 Ma. KGB99-34 K-feldspar has an erratic age spectrum (Fig. 8E) that perhaps indicates excess ^{40}Ar contamination and is not discussed further because it does not provide unambiguous thermochronologic data.

Three minerals from a single sample (KGB99-32a) collected from a Laramide pluton (65.2 ± 0.6 Ma; Brady et al., 2000) located near the west end of the Gold Butte block (Fig. 5) were dated. The muscovite, biotite, and K-feldspar spectra are moderately complex: the muscovite gives an age of 67.8 ± 0.3 Ma for the flattest part of the spectrum (Fig. 8F). All of the steps from the noisy biotite spectrum have a calculated weighted mean age of 48.1 ± 0.5 Ma. The K-feldspar spectrum is characterized by several steps (B–Q; first ~10% of ^{39}Ar released) with ages between ca. 10 and 18 Ma that yield a mean \pm standard deviation (1σ) of 13 ± 3 Ma. Following these initial steps, the spectrum rises abruptly to a slightly complicated ca. 30 Ma part of the spectrum that constitutes the final ~75% of gas release.

PROTEROZOIC COOLING HISTORIES FROM $^{40}\text{Ar}/^{39}\text{Ar}$ ANALYSES

Figure 5 summarizes the new $^{40}\text{Ar}/^{39}\text{Ar}$ dates (squares) in the context of all available thermochronologic data. Ar dates on multiple minerals demonstrate a general age decrease from east to west. We interpret the general age trend to record the passage of the minerals through their nominal closure temperatures (McDougall and Harrison, 1999) of 500 °C for hornblende, 350 °C for muscovite, and 300 °C for biotite. The K-feldspar data will be presented in terms MDD thermochronology, but in general, the youngest apparent ages, represented by initial ages on

¹GSA Data Repository Item 2010080, Appendix 1: $^{40}\text{Ar}/^{39}\text{Ar}$ methods and data and Appendix 2: $^{40}\text{Ar}/^{39}\text{Ar}$ K-feldspar Thermochronology and Multiple Diffusion Domain (MDD) Theory, is available at www.geosociety.org/pubs/ft2010.htm, or on request from editing@geosociety.org, Documents Secretary, GSA, P.O. Box 9140, Boulder, CO 80301-9140, USA.

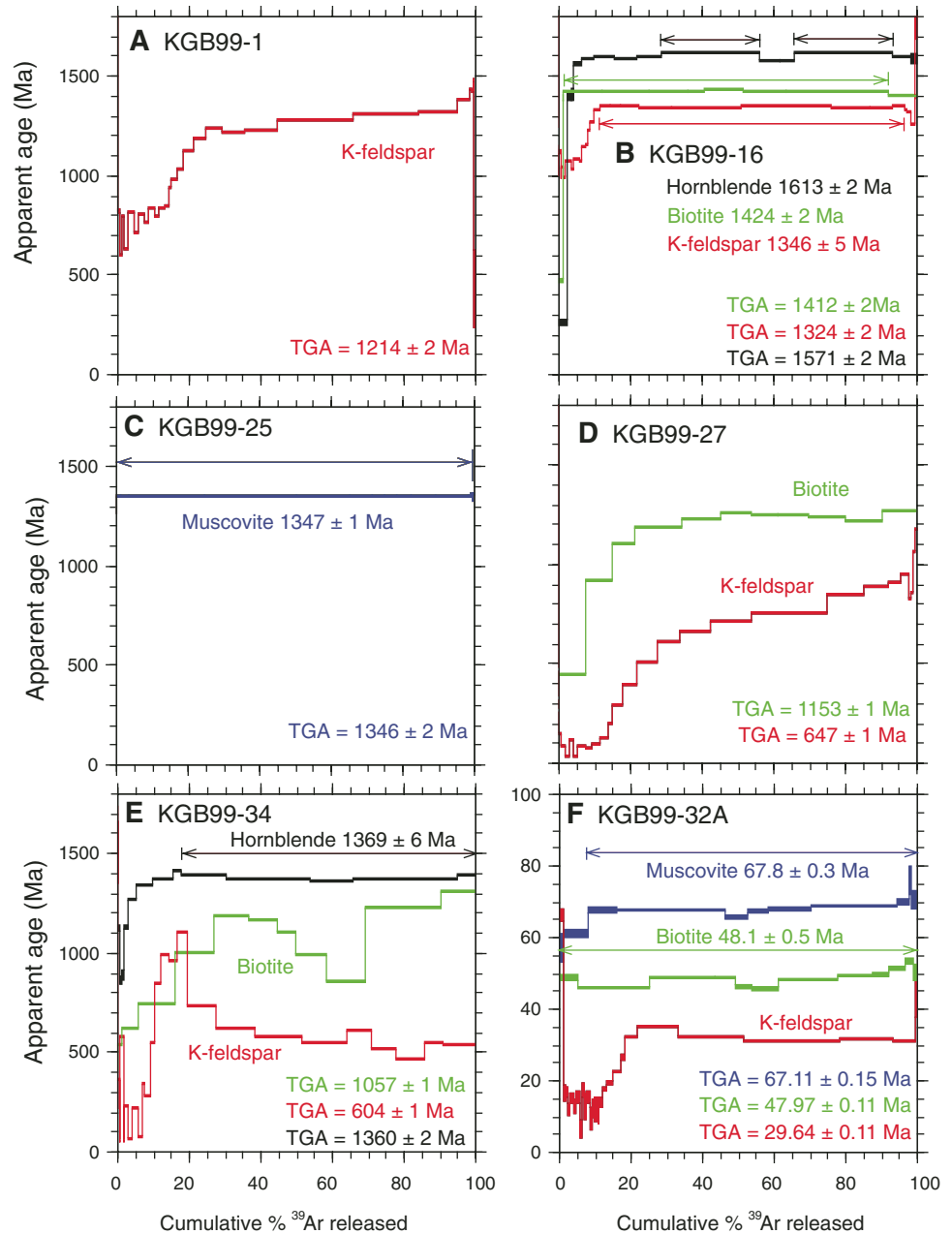


Figure 8. Age spectra samples dated by the $^{40}\text{Ar}/^{39}\text{Ar}$ method. Samples in A–E are Precambrian rocks, whereas data in F are from a Laramide pluton. Minerals are coded by color: red—K-feldspar, green—biotite, black—hornblende, blue—muscovite. TGA—total gas age. Age assignments are justified in the text, but in general, dates corresponding to the steps indicated by the arrows are calculated weighted mean (inverse variance) values and errors are 1σ . Complex spectra are not assigned weighted mean ages. Ages decrease with structural depth and are consistent with a protracted cooling history in the Proterozoic. Muscovite yields an age that is concordant with a U/Pb zircon age at ca. 67 Ma.

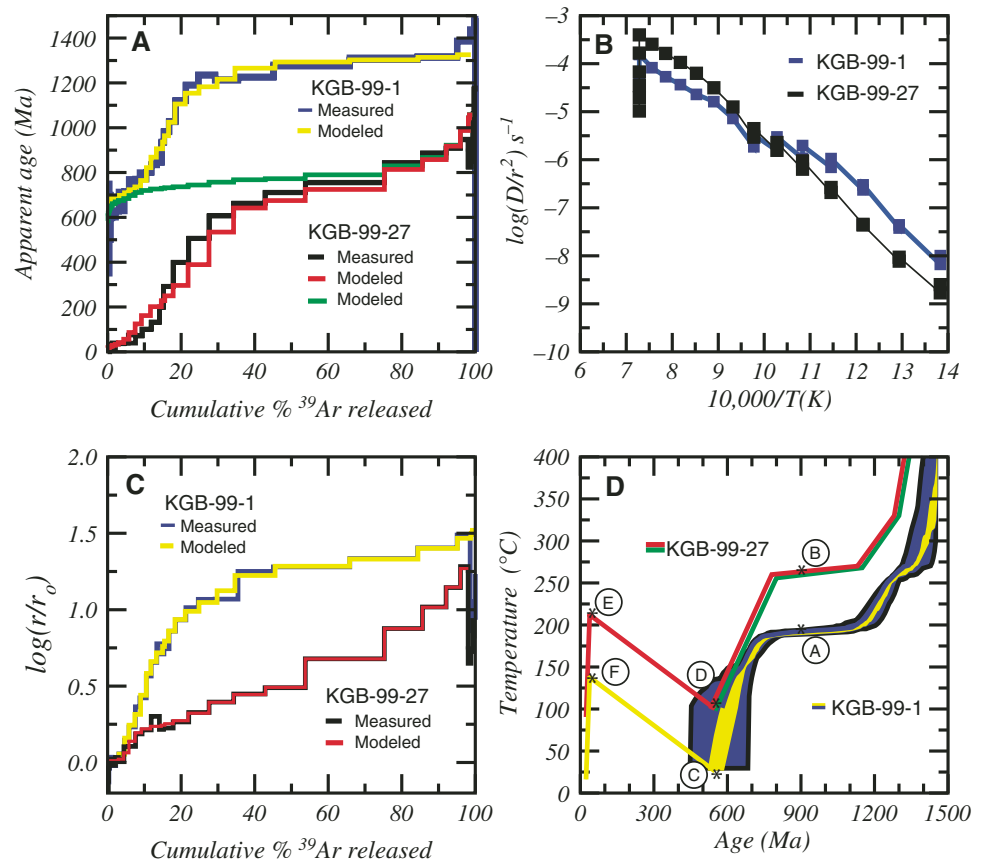
the spectrum, correspond to a closure temperatures of $\sim 175^\circ\text{C}$, whereas the older ages from high-temperature steps correspond to cooling below $\sim 250^\circ\text{C}$ (Appendices 1 and 2 [see footnote 1]).

For most of the block, the combined muscovite and biotite ages from Precambrian rocks get younger from east (1385 Ma muscovite and 1390 Ma biotite) to west (995 Ma muscovite and 1200 Ma biotite), suggesting hotter and deeper crust (in the Proterozoic) exposed in the western part of the block. Most of the mica data indicate cooling through $300\text{--}350^\circ\text{C}$ before ca. 1000 Ma at all exposed paleodepths, but they do not further shed light on the thermal condition of the crust immediately prior to the Miocene. Younger muscovite ages of 70–90 Ma

near the South Virgin–White Hills detachment may suggest Laramide cooling through 350°C (discussed later herein), but they likely are from a structural block with a different cooling history than the rest of the Gold Butte block, as was also suggested by Fitzgerald et al. (1991).

K-feldspar, because of its multiple diffusion domain (MDD) character, can provide a segment of the temperature history between ~ 250 and 175°C for different domains (Lovera et al., 1989). Sample KGB99-1 (Fig. 8A), taken from just beneath the Tapeats Sandstone, has a K-feldspar with an age gradient from ca. 650 to 1300 Ma and is used to estimate the Precambrian thermal history of the highest structural levels (Fig. 9).

Figure 9. Age spectra (A), kinetic data (B, C) and multiple diffusion domain (MDD) thermal histories (D) for KGB99-1 and KGB99-27 K-feldspar. The Precambrian thermal history for KGB99-1 is calculated by standard MDD analysis, assuming cooling only from an originally high temperature. MDD modeling for KGB99-27 is less straightforward due to reheating and argon loss in the Phanerozoic. Because both samples record 900 Ma ages, MDD modeling can estimate their temperatures at this time (points A and B) in graph D. Using the information that the samples differed by 70 °C at this time, and assuming the samples remained at a constant temperature set, the 70 °C is added to the thermal history of KGB99-1 and used to calculate a model spectrum for KGB99-27 that is shown by the green thermal history and green modeled age spectrum. Prior to Tapeats Sandstone deposition, KGB99-1 was at the surface (point C) and KGB99-27 remained 70 °C hotter (point D). KGB99-27 has experienced post-Cambrian argon loss, and the modeled temperature increase to 220 °C between points D and E causes this argon loss, which is represented by the modeled (red) and measured (black) age spectrum gradient (20–600 Ma) over the first ~30% of ^{39}Ar released. Point E equals the maximum pre-Miocene extension temperature, which then decreases below ~100 °C by 17 Ma to be consistent with published apatite fission-track (AFT) data. The thermal history between points C and F represents the equal heating history for KGB99-1 that is implied from KGB99-27, and assuming both samples were always separated in temperature by 70 °C, KGB99-1 would reach 140 °C prior to Miocene extension. This heating to 140 °C does not cause argon loss from KGB99-1 and is thus consistent with the measured spectrum, which does not reveal ages less than ca. 600 Ma.



The age spectrum can be fit with thermal histories that allow cooling only or a reheating history (Appendix 1); however, here we consider the cooling-only models and use the combined methods of Lovera et al. (1989), Quidelleur et al. (1997), Sanders and Heizler (2005), and Sanders et al. (2006) to model the sample. A model age spectrum that closely matches the measured spectrum (Fig. 9A, yellow) is given by a thermal history that suggests two periods of cooling (1300–1150 and 750–600 Ma) with an isothermal (~180 °C) segment from 1150 to 750 Ma (Fig. 9D, yellow-blue). The youngest ages of ca. 600 Ma in the age spectrum (blue, Fig. 9A) indicate that the sample cooled below at least 150 °C by this time and is consistent with the sample position below the Tapeats Sandstone. Importantly, the sample did not experienced Phanerozoic $^{40}\text{Ar}^*$ loss and therefore has not been heated for significant time above 150 °C since 600 Ma.

K-feldspar KGB99-27, from the Gold Butte granite near the west end of the block (Fig. 5), yields an age spectrum that is compatible with significantly higher temperatures relative to KGB99-1 (Fig. 9A, black). This sample reveals substantial Phanerozoic argon loss and is overall much younger than

KGB99-1 and is therefore a sensitive measure of the maximum temperature attained due to burial in the Phanerozoic. MDD modeling of KGB99-27 (Appendix 1; Fig. DR3D) shows that the measured spectrum can be matched with a thermal history passing through ~250 °C at 900 Ma with continued cooling to 200 °C by 600 Ma. Essentially isothermal conditions at 200 °C during the Phanerozoic generate the age gradient observed during the initial 30% of ^{39}Ar release. The sample cools from ~200 °C to below 150 °C between 30 and 15 Ma. Alternate thermal models, which allow reheating (black lines in Fig. DR3D of Appendix 1), also confirm two major conclusions: that this sample was at ~250 °C at 900 Ma and that KGB99-27 attained a maximum Phanerozoic temperature of ~200 °C prior to Miocene extension.

As is generally the case, MDD models can provide a wide range of acceptable thermal histories; however, we can be much more specific about reasonable time-temperature paths when we consider the geological information, relative crustal position between different samples, and other thermochronological constraints. A combination of the MDD information from KGB99-1 and KGB99-27 allows a composite thermal history from ca. 1300 to

20 Ma to be constructed (Fig. 9D). Considering the cooling-only MDD models, sample KGB-99-1 was ~ 70 °C cooler at 900 Ma (point A of Fig. 9D) than KGB-99-27 (point B of Fig. 9D). The accuracy of this temperature offset is mainly a function of the diffusion domain activation energy used in the modeling and has an uncertainty of ~ 25 °C (cf. Lovera et al., 2002). Assuming an intact Gold Butte block, we assume that the thermal histories of these two samples had the same shape, and hence we increase by 70 °C the KGB99-1 temperature model (green line in Fig. 9D). We note that KGB-99-1 had cooled to the surface (10 °C) by Cambrian time (point C of Fig. 9D), and the deeper sample KGB-99-27 is modeled to have been ~ 70 °C hotter (point D of Fig. 9D). Imposing this parallel temperature path onto the kinetic parameters of KGB99-27 yields the green model spectrum presented in Figure 9A, which would be the present-day measured spectrum for KGB99-27 had it not been heated during Phanerozoic burial. Note that sample KGB99-16 K-feldspar (Fig. 8B; Appendix 1, see footnote 1) is also consistent with cooling below 150–200 °C in the Proterozoic, and these data are similar to the Grand Canyon (Timmons et al., 2005) and the Virgin Mountains (Quigley et al., this volume), where K-feldspar give $^{40}\text{Ar}/^{39}\text{Ar}$ ages of 1.4–1.1 Ga. Thermal modeling from these data suggest that basement rocks across this part of the Colorado Plateau–Basin and Range transition cooled through 200 °C in the Mesoproterozoic and have remained cool and in the upper crust since then. This is in contrast with the Arizona transition zone to the south, where Foster et al. (1993) showed 70 Ma K-feldspar ages for Precambrian rocks as the result of Laramide reheating and/or more extensive exhumation of basement rocks (Young, 2001).

Beginning in Tapeats time, both KGB99-1 and KGB99-27 were reheated during deposition and burial by ~ 3 –4 km of Phanerozoic sedimentary rocks. Assuming a range of geothermal gradients from 20 to 30 °C/km, this would result in heating of both samples by ~ 80 –120 °C (red and yellow lines of Fig. 9D). This Phanerozoic burial history is simulated by a linear increase in temperature beginning at 550 Ma where KGB99-27 reaches ~ 210 °C (point E of Fig. 9D) and KGB99-1 reaches ~ 140 °C (point F of Fig. 9D) by 20 Ma. This model heating (Fig. 9D, yellow) does not cause argon loss from KGB99-1 and thus is consistent with the measured spectrum that yields only Precambrian apparent ages. This thermal history is also compatible with the apatite fission-track (AFT) data, which indicate Miocene temperatures less than 110 °C for samples located near the Great Unconformity (Fig. 5). The composite thermal history for KGB99-27 (Fig. 9D, red) yields the red model spectrum (Fig. 9A) that matches well the measured spectrum for KGB99-27. This thermal history is an oversimplification of the burial history, but from a modeling standpoint, the most important constraints are the timing and maximum temperature achieved prior to 20 Ma (point E of Fig. 9D).

These data and models indicate that the pre-Miocene 200 °C isotherm was near the west end of the Gold Butte block, as shown in Figure 5. Based on samples KGB99-27 and -34, this is the shallowest permissible 200 °C isotherm position for Phanero-

zoic (pre-Miocene extension) conditions; rocks east of this line could not have been hotter than ~ 200 °C after ca. 600 Ma for substantial lengths of time without resetting the K-feldspar systems. Note that (U-Th)/He dates of 25 Ma from zircon (closure temperature of ~ 200 –230 °C; Reiners et al., 2002), and 19 Ma from titanite (closure temperature of ~ 200 °C; Reiners et al., 2000) are also generally compatible with this proposed location of the 200 °C isotherm at ca. 20 Ma. In contrast, Reiners et al. (2002) interpreted this isotherm to be ~ 5 km farther east based on (U-Th)/He zircon data (discussed in the following), which we feel is inconsistent with the K-feldspar data.

POST-LARAMIDE THERMAL HISTORY FROM $^{40}\text{Ar}/^{39}\text{Ar}$ K-FELDSPAR DATA

Additional estimates of the post-Laramide but pre-Miocene temperature history at the west (deepest) end of the Gold Butte block come from the $^{40}\text{Ar}/^{39}\text{Ar}$ results of sample KGB99-32a (Fig. 8F). Because the Ar muscovite age is concordant with the published U/Pb monazite age, we can conclude that the pluton was emplaced into crust that was below the muscovite closure temperature (~ 350 °C). The biotite age of ca. 48 Ma is problematic for several reasons. Typically, this biotite age would be suggestive of cooling through ~ 300 °C at ca. 48 Ma, and since the thermal effects related to pluton emplacement would have long before relaxed, it would also suggest that the rocks at a similar crustal position would have been at or above 300 °C between 65 and 50 Ma. However, the biotite and K-feldspar from KGB99-27 that is in a similar (~ 1 –2 km higher) structural position compared to KGB99-32a are not compatible with temperatures above 300 °C between 65 and 50 Ma. This temperature history would not allow Precambrian ages to be recorded by KGB99-27 biotite or K-feldspar. If KGB99-27 and KGB99-32a have similar post-70 Ma thermal histories, then the biotite from KGB99-27 is required to have a higher closure temperature than KGB99-32a biotite. McDougall and Harrison (1999) argued that biotite closure temperature can vary by as much as 100 °C, and therefore if KGB99-27 biotite is ~ 300 °C, the biotite from KGB99-32a could be significantly lower. We do not argue for convenience that KGB99-32a biotite is less retentive than KGB99-27 biotite, we rather favor this argument because the MDD modeling of KGB99-27 K-feldspar, which provides our best quantitative method to assign argon closure temperatures, also does not support ~ 300 °C at 48 Ma. Thus, based on the incompatibility of the two biotites and the K-feldspar results, we suggest that the closure temperature of KGB99-32a biotite is at or below ~ 250 °C, rather than the nominal value of 300 °C.

MDD modeling of KGB99-32a K-feldspar from the pluton can be used to estimate the temperature prior to Miocene extension. Unfortunately, the age spectrum and kinetic data are not ideal from this K-feldspar because the Arrhenius plot (Appendix 2, see footnote 1) does not provide a well-behaved initial linear segment, and therefore the activation energy for argon transport can only be estimated to be 46 kcal/mol (see Lovera

et al., 2002). This limitation leads to uncertainty of the absolute temperature ($\sim\pm 50$ °C) of the model, but it does not significantly affect the shape of the cooling history curve. Additionally, the measured age spectrum is also not ideal because the initial steps yield noisy age data, thereby allowing a wide range of temperature histories between 20 and 10 Ma. The complete MDD results for KGB99-32a are given in Appendix 1 (see footnote 1) and provide the thermal history analyses for both cooling-only and unconstrained models. Figure 10 portrays the MDD data that are most relevant in describing the pre-Miocene extension temperature and perhaps the timing of accelerated cooling. The measured spectrum shown in Figure 10A (green) is modified so that the initial 10% of gas released has an age of 13 ± 3 Ma, which accommodates the scatter of the first several heating steps. This modification allows model thermal histories to be constrained during this time interval, thereby providing a more realistic depiction of thermal history possibilities when considering the age uncertainties. As seen in the cooling models (Fig. 10B), the time of passage below 200 °C has a large uncertainty (red window shows it could be modeled as from 6 to 25 Ma); however, the majority of the thermal models (yellow window, from 12 to 18 Ma) are consistent with other geologic data (AFT data and constraints from the sedimentary record; see following) for accelerated cooling beginning at ca. 17 Ma. Importantly, the models are fairly tightly constrained in indicating maximum temperatures of ~ 225 °C prior to Miocene extension (Fig. 10B).

COMPARISON TO MIOCENE COOLING HISTORIES DERIVED FROM AFT AND (U-Th)/He THERMOCHRONOMETERS

Timing of rapid Miocene extension is well calibrated by the sedimentary rock record in the Gold Butte region. Beard (1996) showed that the 26–18 Ma Rainbow Garden Member of the Horse Mountain Formation was deposited pre-extension (Fig. 6A) and that the 16–14 Ma Thumb Member was deposited synextension. The Miocene cooling history resulting from this extension has been investigated via various lower-temperature thermochronometers. Fitzgerald et al. (1991, 2009) applied AFT studies across the Gold Butte block (ovals of Fig. 5). Reiners et al. (2000) applied (U-Th)/He dating to both titanite (closure temperature of ~ 200 °C) and apatite (closure temperature of ~ 50 – 70 °C) as shown by the triangles in Figure 5, and Reiners et al. (2002) applied (U-Th)/He to zircon (closure temperature of ~ 200 – 230 °C).

The AFT ages (110 °C closure temperature) and (U-Th)/He apatite ages (~ 50 – 70 °C closure temperature) nearly all give similar dates of 14–17 Ma (mean [U-Th)/He apatite age of 15.2 ± 1 Ma; Reiners et al., 2000), synchronous with dates from the synextensional Thumb Member (14–16 Ma; Beard, 1996). This indicates that rocks across most of the block cooled through 60–110 °C during extensional unroofing and cooling of the Gold Butte block starting ca. 17 Ma. There is a good age-depth progression from 50–66 to 34–24 Ma immediately below the uncon-

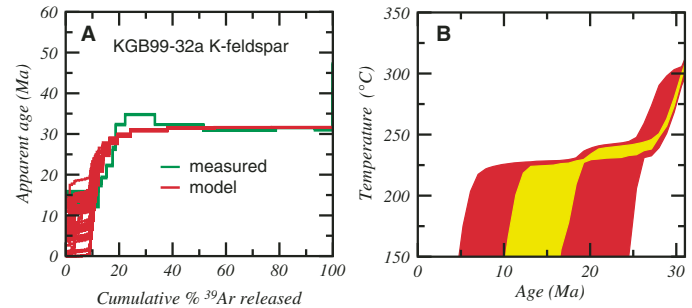


Figure 10. Multiple diffusion domain (MDD) analysis of KGB99-32a K-feldspar. (A) Measured age spectrum (green) and model (red) age spectra. For modeling purposes, the age and uncertainty for the initial noisy 10% of the measured age spectrum are represented by the mean and standard deviation (13 ± 3 Ma) of the steps corresponding to this section of the spectrum. (B) MDD-derived thermal histories reveal a wide distribution of results post-25 Ma due to the age uncertainty; however, the apparent accelerated cooling at 17 Ma is compatible with other published thermochronology data. The isothermal cooling history segment between 17 and 30 Ma at ~ 225 °C represents the pre-Miocene extension temperature and helps constrain the location of the 200 °C isotherm shown on Figure 5.

formity in two transects (Fig. 5; Fitzgerald et al., 1991, 2009), with younger ages toward the west. The transition to 17 Ma ages is within ~ 2 – 3 km of the unconformity in both transects (Fig. 5). The absence of a strong relationship between AFT or (U-Th)/He apatite ages and structural position for most of the deeper portions of the block implies rapid cooling rather than a progressive unroofing as is seen in some core complexes (Foster et al., 1993).

The combined Paleozoic, Mesozoic, and Tertiary section was 3–4 km thick prior to unroofing (Brady et al. [2000] and Reiners et al. [2000] used 2.5 km for the Paleozoic part of the section), which is thick enough to explain temperatures near the unconformity of ~ 75 – 100 °C at a geothermal gradient of ~ 25 °C/km. Thus, based on the change from 34 to 17 Ma in AFT ages, we place the pre-Miocene 100 °C isotherm ~ 2 – 3 km west (~ 1.5 -km-deep below) the Great Unconformity as shown in Figure 5. This also agrees with the present position of the post-Laramide 110 °C isotherm in the eastern Grand Canyon, which is within 1 km below the Paleozoic unconformity (Kelley et al., 2001).

The (U-Th)/He values from apatite and titanite (Reiners, et al. 2000) also help cross-check the inferred positions of the 100 °C and 200 °C pre-20 Ma isotherms (Fig. 5). The titanite data show progressively younger ages, ranging from 192 Ma at upper levels to 19 Ma ages deep in the block. This progression is compatible with progressive erosional denudation of the Colorado Plateau in the early Tertiary (Kelley et al., 2001) and migration downward of the ~ 200 °C isotherm to near the base of the block prior to rapid cooling at 17 Ma. Reiners et al. (2000) placed the 200 °C isotherm at inferred paleodepths of 9.3 km below the unconformity based on the tilted crustal section model and inferred a pre-extensional geothermal gradient of 20 °C/km. Thus, the titanite data are broadly compatible with the K-feldspar Ar data in placing the 200 °C isotherm as shown in Figure 5.

COMPLEXITIES IN THERMOCHRONOLOGIC DATA FROM THE WESTERN GOLD BUTTE BLOCK

Not all the available thermochronology is easily explained by the location of the 200 °C isotherm shown in Figure 5, and, hence, there is some suggestion of a more complex cooling history in the western part of Gold Butte block. In the far southwestern part of Figure 5, Ar muscovite ages are 89–93 Ma and AFT ages are 20–77 Ma, which are both anomalously old for the simple post-17 Ma cooling history under discussion in both structural models. These data may indicate these rocks cooled from 350 to 110 °C in the interval 90–77 Ma, in the Laramide. Fitzgerald et al. (1991) argued that “A more logical explanation is that this sample came from a fragment of the hanging wall that was incorporated into the fault zone and left behind during the tectonic denudation of the block.” The 77 Ma AFT is similar to 70–90 Ma (Laramide) ages from the Lower Granite Gorge (Kelley et al., 2001), Grand Wash Cliffs, and east of the Lake Mead fault in the Lost Basin Range to the south (Fitzgerald et al., 2009), which support the idea that this area may preserve a higher crustal level and older cooling history than of the rest of Gold Butte block.

Additional complexities arise from the 20–25 Ma zircon and titanite (U-Th)/He ages in the central part of the Gold Butte block, which also give some uncertainty about the position of the 200 °C isotherm. These minerals are both inferred to have ~200 °C closure temperatures, such that the far western (U-Th)/He age on zircon (25 Ma) and titanite (19 Ma; sample 98PRGB-4 of Reiners et al., 2000) would be compatible with the 200 °C isotherm at ca. 20 Ma, approximately as shown in Figure 5. However, a kink in the eastward-younging (17–163 Ma) pattern of (U-Th)/He ages led Reiners et al. (2002, their figure 3) to put the 200 °C isotherm several kilometers farther east, at a paleodepth of ~10 km according to model 1 (Fig. 5). This may indicate a segmented (not intact) Gold Butte block, with different segments preserving different (Laramide and early Miocene) cooling histories. This alternative model may also be supported by 20–25 Ma zircon fission-track (ZFT) data in the western part of the Gold Butte block (Bernet et al., 2002). This system has a closure temperature of ~250 °C and also potentially supports a shallower 200 °C isotherm.

Given these caveats, we acknowledge alternate models and the likelihood of a structurally segmented western Gold Butte block. However, for the purposes of this paper, these uncertainties only argue that the 200 °C isotherm may be still shallower than shown in Figure 5, and hence that parts of the western Gold Butte block may have been shallower than shown either in model 1 or model 2 just prior to the pulse of 17–14 Ma extension.

SUMMARY AND DISCUSSION OF ALTERNATIVE STRUCTURAL MODELS BASED ON RESTORED CROSS SECTIONS AND ASSUMED GEOTHERMAL GRADIENTS

The published literature has continued to support the model that the Gold Butte block is one of the thickest, most intact, and best-exposed crustal sections in North America (Wernicke

and Axen, 1988; Fryxell et al., 1992; Fitzgerald et al., 2009, p. 5). As an alternative, Figure 6 shows a structural model and composite cross section constructed by stacking the three cross-section lines shown on Figure 5 and assuming that south-side-up movement on the Gold Butte fault system has juxtaposed slightly different crustal levels within the same detachment system (as discussed herein). In this model, the detachment-bounded basement windows on the Tramp Ridge block (e.g., the Pigs Ear and West Dome) are interpreted to be analogous to the pre-erosion state of the surface of the Gold Butte block. This model involves slip on bedding-parallel weak zones near the Great Unconformity and adds this element to the synchronous slip model of Brady et al. (2000) to provide a more complete description of the extensional history of this region. This structural model suggests relatively modest extension of the cover (~25%; in agreement with estimates of 7%–38% by Brady et al., 2000), but lower extension (~10%) in the basement within the Nevada transition zone, and it models the western part of the block as residing ~8 km below the surface just before extensional exhumation, instead of 15–18 km below the surface.

A synthesis of low-temperature thermochronometers provides good constraints on the positions of the pre-20 Ma 100 °C and 200 °C isotherms in the Gold Butte block. The (U-Th)/He data on titanite is in general agreement with K-feldspar MDD thermal modeling in placing the 18–20 Ma, 200 °C isotherm near the western edge of the Gold Butte block. Apatite fission-track and (U-Th)/He data place the 100 °C isotherm at the east edge of the block, about 2–3 km below the Great Unconformity. The combined data indicate rapid cooling of the block to below 70 °C at 15–17 Ma, in agreement with ages of synextensional sedimentary rocks.

The paleotemperature data can only be converted to paleodepth through evaluation of alternate restored cross sections and assumptions about geothermal gradients. Model 1 *assumes* a pre-Miocene geothermal gradient of 15–20 °C/km (Fryxell et al. [1992] used 15 °C/km; Fitzgerald et al. [2009] and Reiners et al. [2000] used 20 °C/km). The alternative (Model 2) *assumes* 25 °C/km. Either model can explain most of the thermochronology data, including new Ar-Ar data, although data from the southwestern part of the Gold Butte block seem to require some structural segmentation of the block near its western end. The concept of an intact crustal section extending to middle-crustal paleodepths has been fruitful in terms of using the Gold Butte block for calibration of multiple thermochronometers, but additional progress will require integration of structural studies with the thermochronology.

ACKNOWLEDGMENTS

This paper was initiated and reflects detailed mapping by a joint Massachusetts Institute of Technology–University of New Mexico (MIT–UNM) advanced field camp in January 1999. Support from the Crosby Professor fund at MIT for Karlstrom is gratefully acknowledged. We thank MIT faculty

S.A. Bowring and K.X. Whipple for their participation in the field course. Simon Hook of Jet Propulsion Laboratory (JPL) provided the thermal infrared multispectral scanner (TIMS) images and image interpretation. MIT students (including Eric Kirby, Karen Viskupic, and others), and UNM students (including J. Michael Timmons, Colin Shaw, and others) contributed to the mapping and map compilation. The manuscript has benefited from discussions and reviews of early versions of the manuscript by Sue Beard and Keith Howard. Reviews by Robert Brady, Paul Reiners, and Paul Umhoefer are gratefully acknowledged. Ar data were produced at the New Mexico Geochronology Laboratory (www.ees.nmt.edu/Geol/labs/Argon_Lab/NMGRL_homepage.html).

REFERENCES CITED

- Anderson, R.E., and Barnhard, T.P., 1993, Aspects of three-dimensional strain at the margin of the extensional orogen, Virgin River depression area, Nevada, Utah, and Arizona: *Geological Society of America Bulletin*, v. 105, p. 1019–1052, doi: 10.1130/0016-7606(1993)105<1019:AOTDSA>2.3.CO;2.
- Anderson, R.E., Barnhard, T.P., Snee, L.W., 1994, Roles of plutonism, mid-crustal flow, tectonic rafting, and horizontal collapse in shaping the Miocene strain field of the Lake Mead area, Nevada and Arizona: *Tectonics*, v. 13, no. 6, p. 1381–1410.
- Axen, G.J., 1993, Ramp-flat detachment faulting and low-angle normal reactivation of the Tule Springs thrust, southern Nevada: *Geological Society of America Bulletin*, v. 105, p. 1076–1090, doi: 10.1130/0016-7606(1993)105<1076:RFDFAL>2.3.CO;2.
- Axen, G.J., 2007, Research focus: Significance of large-displacement, low-angle normal faults: *Geology*, v. 35, p. 287–288, doi: 10.1130/0091-7613(2007)35[287:RFSOLL]2.0.CO;2.
- Beard, L.S., 1996, Paleogeography of the Horse Spring Formation in relation to the Lake Meade fault system, *in* Beratan, K.K., ed., *Reconstructing the History of Basin and Range Extension Using Sedimentology and Stratigraphy*: Geological Society of America Special Paper 303, p. 27–60.
- Beard, L.S., Anderson, R.E., Block, D.L., Bohannon, R.G., Brady, R.J., Castor, S.B., Duebendorfer, E.M., Faulds, J.E., Felger, T.J., Howard, K.A., Kuntz, M.A., and Williams, V.S., 2007, Preliminary Geologic Map of the Lake Mead 30' × 60' Quadrangle, Clark County, Nevada, and Mohave County, Arizona: U.S. Geological Survey Open-File Report 2007-1010, version 1.0: <http://pubs.usgs.gov/of/2007/1010/> (accessed 23 December 2009).
- Bernet, M., Brandon, M., Garver, J., Reiners, P., and Fitzgerald, P.G., 2002, Determining the zircon fission-track closure temperature: *Geological Society of America Abstracts with Programs*, v. 34, no. 5, p. 18.
- Bohannon, R.G., 1979, Strike-slip faults of the Lake Mead region of southern Nevada, *in* Armentrout, J.M., Cole, M.R., and Terbest, H., eds., *Cenozoic Paleogeography of the Western United States: Pacific Coast Paleogeography Symposium 3*: Los Angeles, Pacific Section, Society of Economic Paleontologists and Mineralogists, p. 129–139.
- Bohannon, R.G., 1984, Nonmarine Sedimentary Rocks of Tertiary Age in the Lake Mead Region, Southeastern Nevada and Northwestern Arizona: U.S. Geological Survey Professional Paper 1259, 72 p.
- Brady, R.J., 2005, Ongoing studies of tilting and uplift in the South Virgin Mountains, Nevada: *Geological Society of America Abstracts with Programs*, v. 37, no. 7, p. 128.
- Brady, R., Wernicke, B., and Fryxell, J., 2000, Kinematic evolution of a large-offset continental normal fault system, South Virgin Mountains, Nevada: *Geological Society of America Bulletin*, v. 112, p. 1375–1397.
- Brumbaugh, D.S., 1987, A tectonic boundary for the southern Colorado Plateau: *Tectonophysics*, v. 136, p. 125–136, doi: 10.1016/0040-1951(87)90335-0.
- Buck, W.R., 1988, Flexural rotation of normal faults: *Tectonophysics*, v. 7, p. 959–973.
- Chamberlain, R.M., 1983, Cenozoic domino-style crustal extension in the Lemitar Mountains, New Mexico: A summary, *in* Chapin, C.E., and Callender, J.F., eds., *Socorro Region II: New Mexico Geological Society Guidebook 34*, p. 111–118.
- Duebendorfer, E.M., and Christensen, C.H., 1995, Synkinematic (?) intrusion of the “anorogenic” 1425 Ma Beer Bottle pluton, southern Nevada: *Tectonics*, v. 14, p. 168–184, doi: 10.1029/94TC02446.
- Duebendorfer, E.M., and Sharp, W.D., 1998, Variation in displacement along strike of the South Virgin–White Hills detachment fault: Perspective from the northern White Hills, northwestern Arizona: *Geological Society of America Bulletin*, v. 110, p. 1574–1589, doi: 10.1130/0016-7606(1998)110<1574:VIDASO>2.3.CO;2.
- Duebendorfer, E.M., Chamberlain, K.R., and Jones, C.S., 2001, Paleoproterozoic tectonic history of the Cerbat Mountains, northwestern Arizona: Implications for crustal assembly in the southwestern United States: *Geological Society of America Bulletin*, v. 113, p. 575–590, doi: 10.1130/0016-7606(2001)113<0575:PTHOTC>2.0.CO;2.
- Dumond, G., Mahan, K., Williams, M.W., and Karlstrom, K.E., 2007, Metamorphism in middle continental crust, Upper Granite Gorge, Grand Canyon, Arizona: Implications for segmented crustal architecture, processes at 25-km-deep levels, and unroofing of orogens: *Geological Society of America Bulletin*, v. 119, p. 202–220, doi: 10.1130/B25903.1.
- Faulds, J.E., and Varga, R.J., 1998, The role of accommodation zones and transfer zones in the regional segmentation of extended terranes, *in* Faulds, J., and Stewart, J., eds., *Accommodation Zones and Transfer Zones: The Regional Segmentation of the Basin and Range Province*: Geological Society of America Special Paper 323, p. 1–46.
- Fitzgerald, P.G., Fryxell, J.E., and Wernicke, B.P., 1991, Miocene crustal extension and uplift in southeastern Nevada: Constraints from fission-track analysis: *Geology*, v. 19, p. 1013–1016, doi: 10.1130/0091-7613(1991)019<1013:MCEAUI>2.3.CO;2.
- Fitzgerald, P.G., Duebendorfer, E.M., Faulds, J.E., and O’Sullivan, P., 2009, South Virgin–White Hills detachment fault system of SE Nevada and NW Arizona: Applying apatite track thermochronology to constrain the tectonic evolution of a major continental detachment fault: *Tectonics*, v. 28, p. TC2001, doi: 10.1029/2007TC002194.
- Flowers, R.M., Wernicke, B.P., and Farley, K.A., 2008, Unroofing, incision, and uplift history of the southwestern Colorado Plateau from apatite (U-Th)/He thermochronometry: *Geological Society of America Bulletin*, v. 120, p. 571–587, doi: 10.1130/B26231.1.
- Foster, D.A., Gleadow, A.J., Reynolds, S.J., and Fitzgerald, P.G., 1993, Denudation of metamorphic core complexes and the reconstruction of the transition zone, west central Arizona: Constraints from apatite fission track thermochronology: *Journal of Geophysical Research*, v. 98, p. 2167–2185, doi: 10.1029/92JB02407.
- Fryxell, J.E., Salton, G.G., Selverstone, J., and Wernicke, B.P., 1992, Gold Butte crustal section, South Virgin Mountains, Nevada: *Tectonics*, v. 11, p. 1099–1120, doi: 10.1029/92TC00457.
- Harrison, T.M., Heizler, M.T., and Lovera, O.M., 1993, In vacuo crushing experiments and K-feldspar thermochronometry: *Earth and Planetary Science Letters*, v. 117, p. 169–180, doi: 10.1016/0012-821X(93)90124-R.
- Hook, S.J., Dmochowski, J.E., Howard, K.A., Rowan, L.C., Karlstrom, K.E., and Stock, J.M., 2005, Mapping variations in weight percent silica measured from multispectral thermal infrared imagery: Examples from the Hiller Mountains, Nevada, USA and Tres Virgenes–La Reforma, Baja California: *Remote Sensing of Environment*, v. 95, no. 3, p. 273–289, doi: 10.1016/j.rse.2004.11.020.
- Howard, K.A., and Bohannon, R.G., 2001, Lower Colorado River: Upper Cenozoic deposits, incision, and evolution, *in* Young, R.A., and Spamer, E.E., eds., *Colorado River Origin and Evolution*: Grand Canyon, Arizona, Grand Canyon Association, p. 101–105.
- Ilg, B., Karlstrom, K.E., Hawkins, D., and Williams, M.L., 1996, Tectonic evolution of Paleoproterozoic rocks in Grand Canyon: Insights into middle crustal processes: *Geological Society of America Bulletin*, v. 108, p. 1149–1166.
- Jackson, G., 1990, Tectonic Geomorphology of the Toroweap Fault, Western Grand Canyon, Arizona: Implications for Transgression of Faulting on the Colorado Plateau: *Arizona Geological Survey Open-File Report 90-4*, 67 p.
- Karlstrom, K.E., Ilg, B.R., Williams, M.L., Hawkins, D.P., Bowring, S.A., and Seaman, S.J., 2003, Paleoproterozoic rocks of the Granite Gorges, *in* Beus, S.S., and Morales, M., eds., *Grand Canyon Geology*: Oxford, UK, Oxford University Press, p. 9–38.
- Karlstrom, K.E., Crow, R.S., Peters, L., McIntosh, W., Raucci, J., Crossey, L.C., Umhoefer, P., and Dunbar, N., 2007, ⁴⁰Ar/³⁹Ar and field studies of Quaternary basalts in Grand Canyon and model for carving

- Grand Canyon: Quantifying the interaction of river incision and normal faulting across the western edge of the Colorado Plateau: *Geological Society of America Bulletin*, v. 119, no. 11–12, p. 1283–1312, doi: 10.1130/0016-7606(2007)119[1283:AAFQ]2.0.CO;2.
- Karlstrom, K.E., Crow, R., Crossey, L.J., Coblenz, D., and van Wijk, J., 2008, Model for tectonically driven incision of the less than 6 Ma Grand Canyon: *Geology*, v. 36, no. 11, p. 835–838, doi: 10.1130/G25032A.1 (with Data Repository item 2008218).
- Kelley, S.A., Chapin, C.E., and Karlstrom, K.E., 2001, Laramide cooling histories of the Grand Canyon, Arizona, and the Front Range, Colorado, determined from apatite fission-track thermochronology, *in* Young, R.A., and Spamer, E.E., eds., *Colorado River: Origin and Evolution*: Grand Canyon, Arizona, Grand Canyon Association, p. 37–42.
- Kirby, E., Karlstrom, K.E., and Andronicus, C., 1995, Tectonic setting of the Sandia pluton: An orogenic 1.4 Ga granite in New Mexico: *Tectonics*, v. 14, p. 185–201, doi: 10.1029/94TC02699.
- Langenheim, V.E., Bohannon, R.G., Glen, J.M., Jachens, R.C., Grow, J.A., Miller, J.J., Dixon, G.L., and Katzer, T.C., 2001, Basin configuration of the Virgin River depression, Nevada, Utah, and Arizona: A geophysical view of deformation along the Colorado Plateau–Basin and Range transition, *in* Erskine, M., Faulds, J., Bartley, J., and Rowley, P., eds., *The Geologic Transition, High Plateau to Great Basin—A Symposium and Field Guide (The Mackin Volume)*: Pacific Section, American Association of Petroleum Geologists, Guidebook 78, p. 205–226. (Also published as Utah Geological Association Publication 30.)
- Lo, Ching-Hua, and Onstott, T.C., 1989, ^{39}Ar recoil artifacts in chloritized biotite: *Geochimica et Cosmochimica Acta*, v. 53, p. 2967–2711.
- Longwell, C.R., 1936, Geology of the Boulder Reservoir floor, Arizona–Nevada: *Geological Society of America Bulletin*, v. 47, p. 1393–1476.
- Longwell, C.R., 1945, Low-angle normal faults in the Basin and Range Province: *American Geophysical Union Transactions*, v. 26, p. 107–118.
- Longwell, C.R., Pampeyan, E.H., Bowyer, B., and Roberts, R.J., 1965, *Geology and Mineral Deposits of Clark County, Nevada*: Nevada Bureau of Mines Bulletin 62, 218 p.
- Lovera, O.M., Richter, F.M., and Harrison, T.M., 1989, $^{40}\text{Ar}/^{39}\text{Ar}$ thermochronology for slowly cooled samples having a distribution of domain sizes: *Journal of Geophysical Research*, v. 94, p. 17,917–17,935, doi: 10.1029/JB094iB12p17917.
- Lovera, O.M., Grove, M., and Harrison, T.M., 2002, Systematic analysis of K-feldspar $^{40}\text{Ar}/^{39}\text{Ar}$ step-heating experiments: II. Relevance of laboratory K-feldspar argon diffusion properties to nature: *Geochimica et Cosmochimica Acta*, v. 66, p. 1237–1255, doi: 10.1016/S0016-7037(01)00846-8.
- McDougall, I., and Harrison, T.M., 1999, *Geochronology and Thermochronology by the $^{40}\text{Ar}/^{39}\text{Ar}$ Method*: New York, Oxford University Press, 269 p.
- Nyman, M.W., and Karlstrom, K.E., 1997, Pluton emplacement processes and tectonic setting of the 1.42 Ga Signal batholith, SW USA: Important role of crustal anisotropy during regional shortening: *Precambrian Research*, v. 82, p. 237–263, doi: 10.1016/S0301-9268(96)00049-6.
- Proffett, J.M., Jr., 1977, Cenozoic geology of the Yerington District, Nevada, and implications for the nature and origin of Basin and Range faulting: *Geological Society of America Bulletin*, v. 88, p. 247–266, doi: 10.1130/0016-7606(1977)88<247:CGOTYD>2.0.CO;2.
- Quidelleur, X., Grove, M., Lovera, O.M., Harrison, T.M., and Yin, A., 1997, Thermal evolution and slip history of the Renbu Zedong thrust, southeastern Tibet: *Journal of Geophysical Research*, v. 102, no. B2, p. 2659–2679.
- Quigley, M.C., 2002, *Tectonic Development of Proterozoic Structures and their Influence on Laramide and Miocene Deformation, North Virgin Mountains, SE Nevada and NW Arizona* [M.S. thesis]: Albuquerque, University of New Mexico, 194 p.
- Quigley, M.C., Karlstrom, K.E., Kelley, S., and Heizler, M., 2010, this volume, Timing and mechanisms of basement uplift and exhumation in the Colorado Plateau–Basin and Range transition zone, Virgin Mountain anticline, Nevada–Arizona, *in* Umhoefer, P.J., Beard, L.S., and Lamb, M.A., eds., *Miocene Tectonics of the Lake Mead Region, Central Basin and Range*: Geological Society of America Special Paper 463, doi: 10.1130/2010.2463(14).
- Reiners, P.W., Brady, R., Farley, K.A., Fryxell, J.E., Wernicke, B., and Lux, D., 2000, Helium and argon thermochronometry of the Gold Butte block, South Virgin Mountains, Nevada: *Earth and Planetary Science Letters*, v. 178, p. 315–326, doi: 10.1016/S0012-821X(00)00080-7.
- Reiners, P.W., Farley, K.A., and Hickes, H.J., 2002, He diffusion and (U-Th)/He thermochronology of zircon: Initial results from the Fish Canyon Tuff and Gold Butte: *Tectonophysics*, v. 349, p. 297–308, doi: 10.1016/S0040-1951(02)00058-6.
- Sanders, R.E., and Heizler, M.T., 2005, Extraction of MDD Thermal Histories from $^{40}\text{Ar}/^{39}\text{Ar}$ K-Feldspar Step Heating Data: New Mexico Bureau of Geology and Mineral Resources Open-File Report OF-AR 26.
- Sanders, R.E., Heizler, M.T., and Goodwin, L.B., 2006, $^{40}\text{Ar}/^{39}\text{Ar}$ thermochronology constraints on the timing of Proterozoic basement exhumation and fault ancestry, southern Sangre de Cristo Range, New Mexico: *Geological Society of America Bulletin*, v. 118, p. 1489–1506, doi: 10.1130/B25857.1.
- Schneider, D.A., Heizler, M.T., Bickford, M.E., Wortman, G.L., Condie, K.C., and Perilli, S., 2007, Timing constraints of orogeny to cratonization: Thermochronology of the Paleoproterozoic Trans-Hudson orogen, Manitoba and Saskatchewan, Canada: *Precambrian Research*, v. 153, p. 65–95, doi: 10.1016/j.precamres.2006.11.007.
- Silver, L.T., Bickford, M.E., Van Schmus, W.R., Anderson, J.L., Anderson, T.H., and Medaris, L.G., Jr., 1977, The 1.4–1.5 b.y. transcontinental anorogenic plutonic perforation of North America: *Geological Society of America Abstracts with Programs*, v. 9, no. 7, p. 1176–1177.
- Timmons, J.M., Karlstrom, K.E., Heizler, M.T., Bowring, S.A., Gehrels, G.E., and Crossey, L.J., 2005, Tectonic inferences from the ca. 1255–1100 Ma Unkar Group and Nankoweap Formation, Grand Canyon: Intracratonic deformation and basin formation during protracted Grenville orogenesis: *Geological Society of America Bulletin*, v. 117, p. 1573–1595, doi: 10.1130/B25538.1.
- Wernicke, B.P., and Axen, G.J., 1988, On the role of isostasy in the evolution of normal fault systems: *Geology*, v. 16, p. 848–851, doi: 10.1130/0091-7613(1988)016<0848:OTROI>2.3.CO;2.
- Wernicke, B.P., Walker, J.D., and Beaufait, M.S., 1985, Structural discordance between Neogene detachments and frontal Sevier thrusts, central Mormon Mountains, southern Nevada: *Tectonics*, v. 4, p. 213–246, doi: 10.1029/TC004i002p00213.
- Williams, M.L., and Karlstrom, K.E., 1997, Looping P - T paths and high- T , low- P middle crust metamorphism: Proterozoic evolution of the southwestern United States: *Geology*, v. 24, no. 12, p. 1119–1122.
- Williams, M.L., Karlstrom, K., Dumond, G., and Mahan, K.H., 2009, Perspectives on the architecture of continental crust from integrated field studies of exposed isobaric sections, *in* Miller, R., and Snoko, A., eds., *Crustal Cross Sections from the Western North America Cordillera and Elsewhere: Implications for Tectonic and Petrologic Processes*: Geological Society of America Special Paper 456, doi: 10.1130/2009.2456(08).
- Young, R.A., 2001, Geomorphic, structural, and stratigraphic evidence for Laramide uplift of the southwestern Colorado Plateau margin of NW Arizona, *in* Erskine, M., Faulds, J., Bartley, J., and Rowley, P., eds., *The Geologic Transition, High Plateau to Great Basin—A Symposium and Field Guide (The Mackin Volume)*: Pacific Section, American Association of Petroleum Geologists Guidebook 78, p. 205–226. (Also published as Utah Geological Association Publication 30.)